Research Square

Preprints are preliminary reports that have not undergone peer review.
They should not be considered conclusive, used to inform clinical practice,
or referenced by the media as validated information.

CCR2-dependent recruitment of SPP1⁺ macrophages promotes noise-induced cochlear inflammation and hearing loss

Ziqi wu
Department of Otolaryngology Head and Neck Surgery, Xijing Hospital, Air Force Medical University
Xinyuan Zhang
Department of Otolaryngology Head and Neck Surgery, Xijing Hospital, Air Force Medical University
Meihao Qi
Department of Otolaryngology Head and Neck Surgery, Xijing Hospital, Air Force Medical University
Xinyv Dong
Department of Otolaryngology Head and Neck Surgery, Xijing Hospital, Air Force Medical University
Zejun gao
Department of Otolaryngology Head and Neck Surgery, Xijing Hospital, Air Force Medical University
Peng Zhang
Department of Otolaryngology Head and Neck Surgery, Xijing Hospital, Air Force Medical University
Xinyv Zhang
Department of Otolaryngology Head and Neck Surgery, Xijing Hospital, Air Force Medical University
Wenyue Wang
Department of Otolaryngology Head and Neck Surgery, Xijing Hospital, Air Force Medical University
Renfeng Wang
Department of Otolaryngology Head and Neck Surgery, Xijing Hospital, Air Force Medical University
Yang Yang
Department of Otolaryngology Head and Neck Surgery, Xijing Hospital, Air Force Medical University
Bei Fan
Department of Otolaryngology Head and Neck Surgery, Xijing Hospital, Air Force Medical University
Jun Chen
Department of Otolaryngology Head and Neck Surgery, Xijing Hospital, Air Force Medical University
Xiaocheng Wang
Center of Clinical Aerospace Medicine, School of Aerospace Medicine, Key Laboratory of Aerospace Medicine of Ministry of Education, Air Force Medical University
Dingjun Zha
zhadjun@fmmu.edu.cn

Department of Otolaryngology Head and Neck Surgery, Xijing Hospital, Air Force Medical University

Research Article

Keywords: Noise-induced hearing loss, Cochlea, Macrophages, SPP1, CCR2, Pyroptosis, Neuroinflammation, Single-cell RNA sequencing

Posted Date: November 25th, 2026

DOI: https://doi.org/10.21203/rs.3.rs-11608155/v1

License: This work is licensed under a Creative Commons Attribution 4.0 International License. Read Full License

Additional Declarations: No competing interests reported.

Title: CCR2-dependent recruitment of SPP1^{+} macrophages promotes noise-induced cochlear inflammation and hearing loss

Author(s)

Ziqi Wu[1,2]*, Xinyuan Zhang[1]*, Meihao Qi[1]*, Xinyv Dong[1], Zejun Gao[1], Peng Zhang[1], Xinyv Zhang[1], Wenyue Wang[1], Renfeng Wang[1], Yang Yang[1], Bei Fan[1]

Corresponding authors

Jun Chen[1#], Xiaocheng Wang[1,2#], Dingjun Zha[1#]

Affiliations

[1] Department of Otolaryngology Head and Neck Surgery, Xijing Hospital, Air Force Medical University, Xi'an, 710032, China

[2] Center of Clinical Aerospace Medicine, School of Aerospace Medicine, Key Laboratory of Aerospace Medicine of Ministry of Education, Air Force Medical University, Xi'an 710032, China.

*These authors contributed equally to this work.

E-mail addresses

Jun Chen: edondongcccj@163.com

Xiaocheng Wang: wxcnose@126.com

Dingjun Zha: zhadjun@fmmu.edu.cn

Corresponding address

Department of Otolaryngology Head and Neck Surgery, Xijing Hospital, Air Force Medical University, 127 Changle West Road, Xi'an 710032, Shaanxi, China

Running title: Cochlear macrophages in noise-induced hearing loss

Abstract

Background Macrophages accumulate in the cochlea after acoustic overstimulation, but their contribution to noise-induced hearing loss (NIHL) remains poorly defined. Here, we investigated the role of macrophages expressing secreted phosphoprotein 1 (SPP1, osteopontin) in NIHL.

Methods We re-analysed public single-cell RNA-sequencing datasets of murine and human inner-ear tissue and performed single-cell RNA sequencing on cochlear immune cells from unexposed and noise-exposed wild-type mice and from noise-exposed *Ccr2* and *Spp1* knockout mice. Hearing function was assessed by longitudinal auditory brainstem response recordings; cochlear hair cells, synapses and macrophages were quantified by immunofluorescence and western blotting; and inflammatory cytokines were measured by enzyme-linked immunosorbent assay. SPP1 or CCR2 was inhibited pharmacologically before noise exposure. Statistical analyses used Fisher's exact test, Wilcoxon rank-sum tests, unpaired two-tailed t-tests and analysis of variance as appropriate.

Results Re-analysis of public murine datasets revealed expansion of a macrophage subset characterized by high expression of *Ccr2* and *Spp1* at three days post-noise exposure. *Ccr2* and *Spp1* knockout mice showed comparable baseline auditory thresholds and smaller noise-induced threshold shifts than wild-type mice, and both deletions preserved cochlear hair cells and ribbon synapses. Cell–cell interaction analysis predicted that $SPP1^{+}$ macrophages communicate with cochlear hair cells and

neurons through SPP1–CD44 and SPP1–integrin pairs and associated SPP1 with a pro-inflammatory macrophage state. In *Spp1*-deficient mice, the expression of pro-inflammatory and pyroptosis-associated molecules was reduced in cochlear macrophages, and cochlear IL-1β and IL-6 levels were attenuated, whereas IL-18 showed a similar but non-significant trend. *Ccr2* knockout reduced the recruitment of $SPP1^+$ macrophages after noise exposure, and pre-exposure pharmacological inhibition of SPP1 or CCR2 partially prevented noise-induced hearing loss.

Conclusions These findings identify CCR2-dependent recruitment of $SPP1^+$ macrophages as a candidate mechanism in NIHL and suggest that targeting the SPP1–CCR2 axis may represent a viable preventive strategy for auditory injury.

Keywords: Noise-induced hearing loss, Cochlea, Macrophages, SPP1, CCR2, Pyroptosis, Neuroinflammation, Single-cell RNA sequencing

Introduction

Noise-induced hearing loss (NIHL) represents a major public health burden worldwide, with an estimated 1.1 billion young individuals at risk of preventable hearing loss due to recreational noise exposure[1]. Despite advances in understanding cochlear pathophysiology, no Food and Drug Administration–approved pharmacological therapies currently exist for NIHL, reflecting the complexity of its underlying mechanisms and the lack of clearly defined therapeutic targets[2, 3].

The cochlea has conventionally been regarded as an immune-privileged organ[4, 5].

However, a growing body of evidence indicates that macrophages play critical roles in the cochlear response to ototoxic and acoustic insults[6, 7]. Under homeostatic conditions, resident macrophages of the murine cochlea, also referred to as microglia, originate from the yolk sac or liver and are involved in synaptic pruning and tissue regression during normal development[8]. Following noise exposure, substantial macrophage recruitment occurs in the cochlea[9, 10], with these cells appearing near the organ of Corti, a region devoid of macrophages under steady-state conditions. This dynamic response suggests that infiltrating or expanded macrophage populations may adopt specialized functions in the injured cochlea. Immune cell activation, particularly of macrophages, has emerged as a key determinant of cochlear injury and repair following acoustic overstimulation[6-8]. However, the functional heterogeneity of cochlear macrophages and the molecular drivers of their phenotypic transitions in response to noise remain incompletely understood.

Recent single-cell transcriptomic studies have begun to unravel the cell-type-specific landscape of the cochlea, including the diversity of cochlear immune cells following noise exposure[11, 12]. In the context of acoustic trauma, macrophages have been shown to exhibit distinct activation states and spatial distribution patterns[6]. Notably, secreted phosphoprotein 1 (SPP1, also known as osteopontin) has been implicated in various inflammatory and tissue remodeling processes across multiple organ systems[13-15]. In the inner ear, proteomic analyses have identified SPP1 as a component of the endolymph, suggesting its potential involvement in cochlear

homeostasis[16]. Furthermore, SPP1-expressing macrophages have been implicated in various pathological contexts, including age-related hearing loss, where elevated SPP1 expression has been observed in the cochlea and auditory cortex[17]. Whether $SPP1^+$ macrophages play a similarly pivotal role in the cochlear response to noise injury remains to be elucidated.

CCR2 is a well-established marker for monocyte-derived macrophages and plays a critical role in mediating their recruitment from the circulation to sites of inflammation[18-20]. In various disease models, including atherosclerosis and atrial fibrillation, CCR2 signaling has been shown to drive the accumulation of pro-inflammatory macrophages that exacerbate tissue injury[18, 19]. However, the contribution of CCR2-mediated macrophage recruitment to cochlear pathology following noise exposure remains poorly defined.

In this study, we investigated the temporal dynamics, origin, and functional contributions of $SPP1^+$ macrophages in a mouse model of NIHL. By integrating single-cell RNA sequencing, genetic knockout models, pharmacological inhibition, and functional assays, we sought to determine whether $SPP1^+$ macrophages represent a pathogenic subset that drives cochlear inflammation and hearing loss. Our findings indicate that $SPP1^+$ macrophages may represent a potential target for preventive intervention in NIHL and provide insight into the inflammatory programs of cochlear macrophages and their contribution to cochlear damage following acoustic overstimulation.

Methods

Animal

All C57BL/6J mice used in this study were obtained from the Laboratory Animal Center of Air Force Medical University. *Spp1* knockout mice (Spp1em1Cya, MGI:7796371; C57BL/6NCya background; deletion of exons 5–8, removing 795 bp of coding sequence corresponding to ~89.5% of the *Spp1* coding region) were purchased from Cyagen Biosciences (Suzhou, China; Cat. No. S-KO-04472). For all experiments involving *Spp1* knockout mice, wild-type controls were C57BL/6N-background littermates from the same breeding colony (i.e. genetically matched to the knockout line), so that substrain background was identical within every *Spp1* experiment. *Ccr2* knockout mice (C57BL/6J-*Ccr2*-KO, strain YDS2572; C57BL/6J background; constitutive knockout generated by ES-cell homologous recombination, with the *Ccr2* coding sequence replaced by a neomycin expression cassette, based on transcript *Ccr2*-203, ENSMUST00000168841.3) were obtained from Wuhan Youdu Biotechnology (Wuhan, China). The *Ccr2* knockout line and the C57BL/6J wild-type controls used in the *Ccr2* experiments are thus both on the C57BL/6J background; the *Spp1* knockout line and its littermate wild-type controls are both on the C57BL/6N background. Genotypes of *Spp1* and *Ccr2* knockout mice were confirmed by PCR; for *Ccr2*, the knockout allele was amplified with primers F1 (5′-CCACAGAATCAAAGGAAATGG-3′) and R1 (5′-CCTTCTATCGCCTTCTTGACG-3′) (390 bp), and the wild-type allele with F1 and R2 (5′-

CACAGCATGAACAATAGCCAAG-3′) (494 bp). Only male mice were used throughout this study, for all genotypes and all experimental groups. Mice were housed under a 12 h light/dark cycle with ad libitum access to food and water. All experimental procedures were approved by the Institutional Animal Care and Use Committee (IACUC) of Air Force Medical University (Protocol No. IACUC-20260039) and were conducted in accordance with the National Institutes of Health (NIH) Guide for the Care and Use of Laboratory Animals. Every effort was made to minimize the number of animals used and to reduce potential suffering. Euthanasia of postnatal and adult mice was performed under deep anesthesia with sodium pentobarbital, following the American Veterinary Medical Association (AVMA) Guidelines for the Euthanasia of Animals (2020 Edition). For mice that underwent auditory brainstem response (ABR) testing, cochleae were collected immediately after the assessment via cervical dislocation under sustained anesthesia.

Noise Exposure

Six-week-old mice were individually placed in cages (9 cm in diameter) and exposed to a 110 dB SPL broadband noise (2–20 kHz) for 2 hours. The noise exposure was conducted within a dedicated sound chamber equipped with a loudspeaker (Model 2450H, JBL, Los Angeles, CA, USA) driven by a power amplifier (AX-500U, Yamaha, Maebashi, Japan). To ensure uniformity of the noise exposure, the sound pressure level was calibrated and verified at multiple positions inside the chamber using a sound level meter (TES 1350A, Taiwan, China).

Single-cell isolation

The organ of Corti, lateral wall, spiral ganglion, and modiolus were dissected from mouse cochleae and digested with papain (20 U/mL; Worthington) in HBSS containing 1 mM L-cysteine and 0.5 mM EDTA for 20 min at 37°C. After gentle trituration, the suspension was filtered through a 40 μm strainer. Total immune cells were isolated using CD45 MicroBeads (Miltenyi Biotec; 130-052-301) according to the manufacturer's protocol. $CD45^+$ cells were eluted and counted before downstream analysis.

Because of the very low immune-cell yield of a single mouse cochlea, cochleae were pooled for each single-cell preparation. Each scRNA-seq sample for the *Spp1* $^{KO/KO}$ group represents a single pool of cochleae from eight mice (i.e., one biological replicate); the WT (baseline) and NE groups each comprised three independently prepared pools (N = 3). Because each KO preparation requires eight animals, three independent KO replicates were not feasible within the scope of this study; this limitation is acknowledged in the Discussion, and the KO scRNA-seq results are presented as descriptive.

Single-cell RNA sequencing (scRNA-seq) analysis

Sorted cells were collected into PBS following the 10× Genomics protocol. The resulting cell suspension was loaded into a Chromium Controller (10x Genomics), and single-cell cDNA libraries were then constructed using Chromium Single Cell 3' Reagent kits (v3) following the manufacturer's protocols. The libraries were quantified and subjected to 150 bp paired-end sequencing on an Illumina NovaSeq 6000 platform (Illumina).

Raw base call files were demultiplexed using the 10x Genomics Cell Ranger pipeline and aligned to the mice transcriptome. Raw gene expression matrices were imported into R (version 4.1.2). The Seurat package was used for cell filtering, data normalization, dimensionality reduction, cell clustering, and the identification of differentially expressed genes. Cells with less than 200 genes and more than 5000 genes or mitochondrial gene content above 10% were excluded for subsequent data analysis. 'FindVariableFeatures' was used to identify the top 2000 most hypervariable genes, and these genes were selected for principal component analysis (PCA) and linear dimension reduction. The original Louvain algorithm (FindClusters) with a clustering resolution of 0.6 was performed to cluster the cells. Differentially expressed genes were identified using a Wilcoxon rank-sum test with a P value cutoff of 0.05 and a log(fold change) threshold of 0.25. Cell types were allocated to each cluster using the known marker genes as described previously. For the re-analysis of the public dataset GSE167078 (Fig. 1), the quality-control thresholds reported in the original publication were applied (nFeature_RNA > 500 and < 6,000; nCount_RNA < 40,000; percent.mt < 7%).

The RNA-seq data have been deposited in the GEO database under accession number GSE346691. The publicly available datasets GSE167078 (Milon et al. [12]) and GSE213796 (van der Valk et al. [21]) were re-analyzed in this study.

Auditory Brainstem Response (ABR) Measurement

Mice were anesthetized via intraperitoneal injection of sodium pentobarbital (50 mg kg^{-1}) and placed on a temperature-controlled heating pad within a sound-attenuating,

electrically shielded chamber. Frequency-specific auditory responses were recorded using a Tucker-Davis Technologies (TDT, Alachua, FL, USA) RZ6 system. Subdermal needle electrodes were positioned at the vertex (midline suture), the ipsilateral mastoid region, and the tail base (ground). Acoustic stimuli (15 ms tone bursts with 1 ms rise/fall time) were generated, and responses were recorded using TDT System III hardware and SigGen/BioSig software. The ABR signals were filtered (high-pass: 300 Hz; low-pass: 3 kHz). Hearing thresholds were determined at click, 8, 16, 24, and 32 kHz by initially decreasing stimulus intensity in 10-dB steps and then in 5-dB steps near threshold until a reproducible waveform was no longer detectable. The threshold was defined as the lowest stimulus intensity level at which a distinct, repeatable wave pattern could be visually identified. All ABR measurements were performed by a single experienced experimenter, and threshold determinations were made by an expert blinded to the experimental conditions. Each experimental group comprised six mice, and only male mice were used. ABR measurements were longitudinal: the same cohort of mice was recorded before noise exposure and again at 14 days post-exposure, with each animal serving as its own baseline control; paired statistical tests were therefore used for within-cohort comparisons. Both absolute thresholds (dB SPL) and threshold shifts are reported.

Immunofluorescence staining

Cochleae were removed from mice treated as described above and fixed with 4% paraformaldehyde at 4 °C for ^{12} h. After decalcification by soaking in 10% EDTA, the

basilar membrane was removed. After being washed with 1× PBS (Cytiva; SH30256.01), the cells were treated with 0.5–1% Triton X-100 (Biosharp, BS084) at room temperature for 10 min and blocked with 5% BSA at 37 °C for 45 min. Primary antibodies were diluted with an antibody diluent. Fifty microliters of diluted antibodies were added to each cochlear tissue sample. After incubation at 4 °C for 48 h, the samples were washed with 1× PBS, a fluorescent secondary antibody was added, the samples were wrapped with tin foil in the dark, incubated at room temperature for 24 h, rinsed with 1× PBS, and incubated with DAPI (1:1000; Sigma; 28718-90-3) or phalloidin (1:200; Abcam; ab176753). After the samples were washed, they were placed on a slide and observed under a laser confocal microscope. ImageJ (Fiji; 1.54d) was used to perform a semiquantitative analysis of the laser confocal images. Scale bars in all immunofluorescence images represent 10 μm. The following primary antibodies were used: rabbit polyclonal anti-myosin 7a (1:1000; Proteus Biosciences; 25-6790), goat polyclonal anti-SPP1 (1 μg/mL; R&D Systems; AF808-SP), mouse monoclonal anti-Iba1 (1:800; ASIS; OB-IF-Fr-HH01), rabbit polyclonal anti-Iba1 (1:200; Affinity; DF6442), mouse monoclonal anti-CtBP2 (1:200; BD Biosciences; 612044), rabbit polyclonal anti-CD68 (1:200; Affinity; DF7518). The following secondary antibodies were used for detection: donkey anti-rabbit IgG (1:400; Invitrogen; A31573), donkey anti-rabbit IgG (1:400; Invitrogen; A21207), donkey anti-rabbit IgG (1:400; Invitrogen; A21206), donkey anti-goat IgG (1:400; Invitrogen; A11058), donkey anti-mouse IgG (1:400; Invitrogen; A11005), and donkey anti-mouse IgG (1:400; Invitrogen; A32766).

Western Blotting

The cochlear tissue was placed in RIPA lysis buffer (Glpbio; GK10023) containing PMSF (1:100; Glpbio; GC10477) and a protease inhibitor cocktail (1:100; Glpbio; GK10014). The protein concentration was measured using a BCA protein assay kit (Glpbio; GK10009). A total of 30 μg of each protein sample was separated on 4–12% SDS–PAGE gels. After electrophoresis, the proteins were transferred to polyvinylidene difluoride membranes. Membranes were blocked with 5% non-fat milk in TBST for 1 h at room temperature, incubated with primary antibodies overnight at 4 °C, and then with secondary antibodies at 37 °C for 1 h. After three washes, the bands were visualized via a chemiluminescence substrate (Millipore, WBKLS0500) and analyzed using ImageJ software. The following primary antibodies were used: goat polyclonal anti-SPP1/osteopontin (0.1 μg/mL; R&D Systems; AF808-SP) and mouse monoclonal anti-β-actin (1:1000; Abcam; ab8226). The following secondary antibodies were used: HRP-conjugated AffiniPure goat anti-rabbit (or anti-mouse) IgG (1:5000; Proteintech; SA00001-2, SA00001-1), and HRP-conjugated rabbit anti-goat IgG (Affinity; 1:10000). Because the protein yield from a single mouse cochlea is limited, lysates from three mice (six cochleae) were pooled for each sample lane. Western blotting was repeated three times independently, with independently prepared samples, gels and membranes. Molecular-weight markers were Vazyme MP201 (180, 130, 100, 70, 55, 40, 35, 25, 20, 15 and 12 kDa). Full-length, uncropped scans of all membranes, including the marker

lanes and lane assignments, are provided in the supplementary uncropped-blot file.

The band intensities of SPP1 were quantified using ImageJ software. Relative protein expression was calculated by normalizing SPP1 intensity against the corresponding β-actin intensity from the same sample. Fold change was calculated relative to the control group.

Flow Cytometry and Cell Sorting

Fresh anticoagulated blood was centrifuged at 400–500 ×g for 5 minutes, and the supernatant was discarded. The cell pellet was resuspended in 6–10 volumes of red blood cell (RBC) lysis buffer, gently mixed, and incubated at room temperature for 1–2 minutes. Following lysis, the sample was centrifuged again (400–500 ×g, 5 minutes), and the red supernatant was discarded. This lysis step was repeated once. The remaining cells were washed twice with 5 ml phosphate-buffered saline (PBS) to obtain the final cell suspension for analysis.

The cell pellet was divided into two aliquots. One aliquot was used for cell counting. The other was stained for flow cytometry. First, cells were incubated with an Fc receptor blocking reagent for 10 minutes at room temperature. Subsequently, the following fluorochrome-conjugated antibodies were added and incubated for 30 minutes at 4°C in the dark: anti-CCR2 (3 μL; Biolegend, Cat# 150627), anti-CD11b (2 μL; Biolegend, Cat# 101229), and anti-F4/80 (2 μL; Biolegend, Cat# 111603). After staining, cells were resuspended in 1 mL of flow cytometry staining buffer, centrifuged, and the

supernatant was discarded. For intracellular staining of SPP1, cells were fixed and permeabilized using the FIX & PERM™ Cell Permeabilization Kit (Thermo Fisher Scientific). Briefly, 100 µL of Medium A (fixation reagent) was added, cells were gently resuspended, and incubated for 20 minutes at room temperature in the dark. Cells were then washed with 1 mL of staining buffer and centrifuged. Next, 100 µL of Medium B (permeabilization reagent) and 1 µL of anti-SPP1 antibody (Sanying Biotechnology, Wuhan, China, Cat# cl488-22952) were added, followed by incubation for 30 minutes at room temperature in the dark. Finally, cells were washed with 1 mL of staining buffer and centrifuged. Stained samples were analyzed on a flow cytometer. Data processing and graphical representation were performed using FlowJo software (version 10.8.1).

Enzyme-linked immunosorbent assay (ELISA)

Cochlear tissues were collected and homogenized in ice-cold saline (9 volumes per gram of tissue) to prepare 10% (w/v) tissue homogenates. The homogenates were centrifuged at 2500–3000 rpm for 10 min at 4°C, and the supernatants were collected for subsequent analysis. Concentrations of IL-1β, IL-6, and IL-18 were measured using commercially available ELISA kits according to the manufacturers' protocols (IL-1β: EK201B, Lianke Bio; IL-6: EK206, Lianke Bio; IL-18: EK218, Lianke Bio). Absorbance was read at 450 nm using a microplate reader, and cytokine levels were calculated based on standard curves.

Drug Administration

For the SPP1 inhibitor group, C57BL/6 mice received a single intraperitoneal injection

of an SPP1 inhibitor (MCE, HY-146064) at a dose of 70 mg kg^{-1}, administered one day prior to noise exposure. For the CCR2 inhibitor group, C57BL/6 mice were administered a CCR2 inhibitor (MCE, HY-18611) via daily intraperitoneal injection at a dose of 100 mg kg^{-1} for 10 consecutive days, commencing 10 days before noise exposure. Both inhibitors were first dissolved in dimethyl sulfoxide (DMSO) to prepare stock solutions according to the manufacturer's instructions and were subsequently diluted in sterile physiological saline to obtain the final working concentrations. Mice in the control group received intraperitoneal injections of an equivalent volume of the DMSO–saline vehicle on the same schedule as the inhibitor-treated groups.

Statistical analysis

All data were analyzed using GraphPad Prism (version 9.0) and R software (version 4.5.2). Data are presented as mean ± standard error of the mean (SEM) unless otherwise indicated. Comparisons between two groups were performed using an unpaired two-tailed Student's t-test, except where a paired design was used (longitudinal ABR recordings; see Methods). For comparisons involving more than two groups, one-way or two-way analysis of variance (ANOVA) was used, followed by Tukey's or Sidak's post hoc test for multiple comparisons, as appropriate. For ABR threshold shift analysis, two-way repeated-measures ANOVA was applied to account for frequency and time factors. For single-cell composition analyses, cellular abundance was expressed as a proportion of the total recovered cells (normalized counts), and all comparisons were performed on these normalized proportions rather than on raw counts. The number of

biological replicates (n) is stated in each figure legend; n refers to the number of independent animals unless otherwise specified.

For single-cell RNA sequencing data, differential gene expression analysis was performed using the Wilcoxon rank-sum test, with a significance threshold of $P < 0.05$ and a $\log_2$(fold change) threshold of 0.25; P values were adjusted for multiple testing using the Benjamini–Hochberg procedure. CellChat [22] was used to infer ligand–receptor interactions and cell–cell communication networks, with significance determined by permutation testing (1,000 permutations). For flow cytometry and immunofluorescence quantification, at least three independent biological replicates were analyzed per condition. Correlation analyses between single-cell gene expression profiles were performed using Spearman's rank correlation coefficient, chosen because single-cell expression data are zero-inflated and non-normally distributed; both R and P values are reported. For single-cell data, the proportion of cells expressing a given gene denotes the fraction of cells within the indicated population in which at least one transcript of that gene was detected.

All experiments were repeated at least three times independently unless otherwise specified. Statistical significance was defined as $p < 0.05$, with significance levels indicated as $*p < 0.05$, $**p < 0.01$, $***p < 0.001$, and $****p < 0.0001$. Blinding was applied during ABR threshold measurement and immunofluorescence image quantification to minimize bias. Animals were allocated to experimental groups using a computer-generated random number sequence generated by an investigator who was

not involved in the subsequent data acquisition. Sample sizes were determined from effect sizes observed in pilot experiments and in previously published noise-exposure studies from our laboratory, and were sufficient to detect the differences reported here at a two-sided α of 0.05. Pre-established exclusion criteria were applied before analysis: animals that died or showed signs of severe illness before the experimental endpoint, and samples with technically failed recordings, were excluded and replaced; no outliers were removed from any dataset after analysis.

Results

A *Spp1*-high macrophage cluster expands in the cochlea after noise exposure

We analyzed a publicly available scRNA-seq dataset of cochlear immune cells reported by Milon et al. [12] (GSE167078), generated from mice at baseline (pre-noise) and at 3, 7, and 14 days after exposure to 105 dB broadband white noise for 2 hours. After quality control filtering (nFeature_RNA > 500 and < 6,000, nCount_RNA < 40,000, percent.mt < 7%), 1,556 cells were initially retained. Following doublet removal, 1,258 high-quality immune cells were obtained for downstream analysis. These cells were clustered into 13 distinct clusters (designated 0–12) and annotated using established lineage markers [19, 23, 24] (Fig. 1A, B; Fig. S1A), yielding

363 populations of 596 neutrophils (*Ly6g*, *Lcn2*), 379 B cells (*Cd79b*, *Cd79a*, *Cd19*), 187
364 T cells (*Cd8a*, *Cd8b1*), and 96 macrophages (*Cd68*, *Cd14*, *Aif1*) (Fig. 1A, B). For the
365 cell–cell communication analysis reported below (Fig. S2), the same published atlas
366 was used without restriction to $CD45^+$ immune cells, so that putative interactions
367 involving supporting cells, hair cells and neurons could also be evaluated.
368 We observed a distinct temporal distribution pattern of cochlear macrophages following
369 noise exposure. To control for the possibility that the apparent decline in macrophage
370 numbers at later time points simply reflected a smaller total number of cells recovered,
371 macrophage abundance was normalized to the total number of recovered immune cells
372 at each time point rather than expressed as absolute counts. On this normalized basis,
373 macrophages (Clusters 10 and 11 combined) accounted for 9.3% of recovered cochlear
374 immune cells at baseline, 8.4% at 3dNE, 4.7% at 7dNE, and 5.7% at 14dNE (Fig. 1C).
375 Dimensionality reduction revealed that macrophages segregated into two distinct
376 clusters, designated Cluster 10 and Cluster 11 (Fig. 1A, B). The composition of the
377 macrophage compartment changed markedly after noise exposure: Cluster 11
378 accounted for 22.2% of macrophages at baseline, 63.0% at 3dNE, 53.8% at 7dNE and
379 40.0% at 14dNE (Fig. 1D). Macrophages recovered at 3dNE had approximately six-
380 fold higher odds of belonging to Cluster 11 than those at baseline (Fisher's exact test, P
381 = 0.0014; the overall Cluster 10/11 × time-point association was also significant, P =
382 0.0071), whereas macrophages from baseline were distributed mainly within Cluster 10
383 (77.8%). These findings indicate that the *Spp1*-high Cluster 11 macrophage

subpopulation expands acutely after noise exposure, warranting further investigation of its functional role.

Enrichment of phagocytosis- and pyroptosis-related pathways in the SPP1-expressing macrophage cluster

To explore the functional differences between these two macrophage clusters, we performed differential gene expression analysis between Cluster 10 and Cluster 11 macrophages. Gene Set Enrichment Analysis (GSEA) of Kyoto Encyclopedia of Genes and Genomes (KEGG) pathways revealed that Cluster 11 macrophages exhibited significant enrichment of gene sets associated with lysosomal activation, efferocytosis (phagocytic clearance of apoptotic cells), Staphylococcus aureus infection, and monocyte recruitment (Fig. 1E). In contrast, Cluster 10 macrophages were enriched for gene sets related to cell adhesion molecules (CAMs) (adjusted $P = 0.0067$) and the PI3K–Akt signaling pathway (adjusted $P = 0.024$), with additional nominal enrichment of ECM–receptor interaction, Th17 cell differentiation, and C-type lectin receptor signaling (nominal $P < 0.05$; not significant after multiple-testing correction) (Fig. 1E). These results indicate that Cluster 10 and Cluster 11 macrophages differ not only in the expression of individual effector molecules but also in their underlying signaling programs.

Among the top 20 differentially expressed genes (DEGs) between Cluster 10 and Cluster 11 macrophages, the most highly expressed genes included *C1qa*, *C1qb*, *C1qc*, *Trem2*, *Spp1*, and *Apoe* (Fig. 1F). Among these DEGs, *Spp1* expression was

predominantly confined to the macrophage population among recovered cochlear immune cells (Fig. 1G, H). Further analysis revealed significant upregulation of *Il1b* and *Nlrp3* expression in macrophages following noise exposure (Fig. 1I). Moreover, IL-1β expression differed significantly, albeit modestly, between *Spp1*$^{+}$ and *Spp1*$^{-}$ macrophage subsets (Fig. 1J).

Through analysis of a publicly available single-cell RNA-sequencing dataset (GSE213796) derived from human inner ear tissue [21], we identified SPP1^{+} macrophages whose gene-expression profile correlated significantly, though modestly, with that of their murine counterparts (Fig. S3A–F); these cross-species data are considered further in the Discussion.

Based on our analyses of these public datasets, we hypothesized the existence of a specialized macrophage subpopulation characterized by high SPP1 expression following noise exposure, and further speculated that this subpopulation may contribute to the pathology of noise-induced hearing loss (NIHL).

SPP1 expression in the cochlea and macrophages at selected time points following noise exposure

To investigate the presence of SPP1^{+} macrophages in the cochlea after noise exposure, we exposed 6-week-old C57BL/6J mice to 110 dB SPL broadband white noise (2–20 kHz) for 2 h to establish a NIHL model [25, 26]. Auditory assessment revealed permanent threshold shifts in auditory brainstem responses (ABRs) at 14 days post-noise exposure (Fig. S4C). Histological analysis confirmed irreversible damage,

including significant loss of hair cells and ribbon synapses (Fig. S4A, B, D, E).

Western blot analysis demonstrated an approximately two-fold increase (mean 2.0 versus 1.0) in cochlear SPP1 protein levels at 3 days post-noise compared with baseline (Fig. 2D, E). Immunofluorescence staining of cochlear basilar membrane whole mounts at baseline and at 1, 3, and 14 days post-noise (Fig. 2A) confirmed the presence of $SPP1^+$ macrophages, which were predominantly localized around the hair cell region. The density of $SPP1^+$ macrophages was quantified as 2–4 cells per 100 μm of basilar membrane at 1 day and 3–5 cells per 100 μm at 3 days post-noise, with a parallel increase in relative SPP1 fluorescence intensity (Fig. 2B, C). In contrast, virtually no $SPP1^+$ macrophages were detected in the apical, middle, or basal turns of control cochleae or at 14 days post-noise (Fig. 2B). Collectively, these findings support the presence of a distinct $SPP1^+$ macrophage subpopulation in the cochlea at 3 days post-noise exposure.

CCR2 signaling mediates the recruitment of $SPP1^+$ macrophages after noise exposure

We analyzed the expression of *Ccr2* and *P2ry12* in the noise-exposed cochlear $SPP1^+$ macrophage subpopulation from GSE167078. More than 80% of macrophages with high *Spp1* expression were CCR2-positive, whereas macrophages with high *P2ry12* expression were predominantly *Spp1*-negative (Fig. S1B). To quantify these relationships, we computed Spearman's rank correlation between *Spp1* and *Ccr2* expression ($R = 0.42$, $P = 0.0017$; $n = 46$) and between *Spp1* and *P2ry12* expression (R

= −0.21, P = 0.084; n = 46) at the single-cell level in all macrophages from the noise-exposed cochlea (i.e. without pre-selecting *Spp1*$^{+}$ cells, to avoid range restriction) (Fig. 3D). These relationships are consistent with SPP1^{+} macrophages arising from CCR2^{+} circulating monocytes rather than from resident *P2ry12*-expressing microglia.

Given the high *Ccr2* signature within SPP1^{+} macrophages, we speculated that these pathogenic macrophages may originate from circulating monocytes rather than local resident microglia. We therefore performed flow cytometry on peripheral blood to dynamically monitor monocyte/macrophage populations after noise exposure, using CD11b and F4/80 to label monocyte/macrophage-like cells. The proportion of these cells in the blood increased significantly as early as 1 h post-noise, peaked at 12 h, and returned to near-baseline levels by day 1. Notably, the proportion of SPP1 and CCR2 double-positive cells, identified by intracellular staining in the same flow cytometric analysis, increased markedly at 1 h post-noise and normalized by 12 h (Fig. 3A-C).

To further explore the role of CCR2 signaling following noise exposure, we subjected *Ccr2* $^{KO/KO}$ mice on a C57BL/6J background to the same noise paradigm. *Ccr2* $^{KO/KO}$ mice exhibited normal baseline hearing (Fig. 4B); the auditory and histological consequences of *Ccr2* deletion after noise exposure are presented together with those of *Spp1* deletion below (Fig. 5).

To assess the impact of CCR2 deficiency on the abundance of SPP1^{+} macrophages in the cochlea, we harvested cochlear tissues at 3 days after noise exposure from naive WT mice, noise-exposed WT mice, and noise-exposed *Ccr2* $^{KO/KO}$ mice. Cochlear immune cells were isolated by magnetic bead sorting and analyzed by single-cell RNA

sequencing (GSE346691; Fig. 6A). Two independent biological replicates of noise-exposed WT samples (WT-NE1 and WT-NE2) were analyzed, and their data are presented in Fig. 6B (rather than a comparison between naive WT and noise-exposed WT groups). When cellular abundance was expressed as a proportion of the total recovered cells at each time point (normalized counts) rather than as raw counts, the proportions of macrophages and neutrophils recovered from the *Ccr2* $^{KO/KO}$ group were lower than those from noise-exposed WT mice (Fig. 6B). In the same comparison, the number of SPP1^{+} macrophages was lower in *Ccr2* KO/KO mice than in noise-exposed WT controls, although this difference did not reach statistical significance in the single-cell data (Fig. 6C). Fig. 6C compares only noise-challenged groups, because the analysis focused specifically on noise-induced macrophage alterations. Immunofluorescence staining of cochlear basilar membranes further validated the significant reduction of SPP1^{+} macrophages surrounding hair cells in *Ccr2* $^{KO/KO}$ mice (Fig. 6D–F). Macrophage clustering and differential gene analyses before and after noise exposure demonstrated that cochlear *P2ry12*$^{+}$ microglia-like cells barely expressed *Spp1*, whereas noise-stimulated SPP1^{+} macrophages exhibited negligible expression of proliferation-related genes (Fig. 6G).

Frequent predicted cell–cell communication of SPP1^{+} macrophages after noise exposure

Having established that CCR2-recruited SPP1^{+} macrophages accumulate in the noise-damaged cochlea, we next asked through which signaling routes these cells could influence the cochlear parenchyma. Because global measures of inferred communication scale with the number of cells recovered per cluster, overall interaction counts carry little information on their own, and we therefore did not interpret them. Instead we confined the analysis to the SPP1 pathway, in which the sending

compartment is fixed by ligand expression rather than by network inference: within our dataset *Spp1* expression is restricted to the SPP1^{+} macrophage subset (Fig. 1G, H; Fig. S2A).

We then asked which cochlear cells are positioned to receive this signal. The predicted SPP1 receptors, CD44 and the integrin pair ITGAV+ITGB1, were expressed by cochlear supporting cells, hair cells and neurons, as well as by neutrophils, T cells, B cells and macrophages themselves (Fig. S2B). Among the ligands detected in the structural compartments, several showed increased expression after noise exposure, whereas *Spp1* itself remained confined to the SPP1^{+} macrophage subset (Fig. S2C; Fig. 1G, H). Because macrophages also express CD44 and the integrin subunits, these predictions raised the possibility that SPP1 acts back on macrophages in an autocrine manner, in addition to acting on cochlear structural cells. We therefore quantified the co-expression of the relevant ligands and receptors within macrophages (Fig. 7A–C).

Altered expression of phagocytosis- and pro-inflammation-associated molecules in macrophages of *Spp1* $^{KO/KO}$ mice after noise exposure

Our earlier KEGG enrichment analysis of the scRNA-seq data (Fig. 1E) highlighted strong pyroptosis-pathway signatures within the SPP1^{+} macrophage cluster. We hypothesized that SPP1 may promote a pyroptosis-associated inflammatory state in macrophages and the subsequent release of pro-inflammatory mediators in the noise-injured cochlea. To test this, we compared pyroptosis-related signatures and cochlear cytokine levels between WT and *Spp1* $^{KO/KO}$ mice.

Analysis of ligand and receptor expression in macrophages before and after noise exposure revealed upregulation of molecules associated with a pro-inflammatory macrophage state, including *Fn1* [27-29] and *Mif* [30, 31], whereas *Lgals9* [32, 33] remained essentially unchanged (Fig. 7A). Macrophages also showed high expression of the receptors *Cd44*, *Ccr2* and *Tyrobp* (Fig. 7B).

In *Spp1* $^{KO/KO}$ mice, *Fn1* expression was reduced, whereas *Mif* expression increased significantly and *Lgals9* expression was almost unchanged (Fig. 7A). Expression of the receptors *Ccr2* and *Tyrobp* was also decreased (Fig. 7B). *Tyrobp* expression increased after noise exposure; although *Spp1* knockout lowered overall *Tyrobp* expression, the levels remained substantially above the no-noise baseline. Thus, *Spp1* deletion did not uniformly suppress these molecules but rather shifted the balance between them.

We found that overall *Trem2* expression in macrophages increased after noise exposure; in *Spp1* $^{KO/KO}$ mice, macrophage *Trem2* expression was slightly but statistically significantly lower than in noise-exposed WT mice, although the effect size was small (mean 0.080 vs 0.099; Wilcoxon P = 0.00012) (Fig. 7C). Our prior sequencing results indicated that the SPP1^{+} macrophage subpopulation is enriched in pathways related to efferocytosis (Fig. 1E).

Together with the receptor changes described above, these results indicate that SPP1 shapes the ligand and receptor profile of cochlear macrophages after noise exposure, although the mechanisms through which it does so remain to be determined.

Reduced pyroptosis-associated signatures and inflammatory cytokine levels in

536 ***Spp1*-knockout mice following noise exposure**

537 Analysis of the single-cell data showed that, among the cell-death molecules examined,
538 expression of the pyroptosis-related molecules caspase-1 and caspase-11 (encoded by
539 *Casp11*) was reduced in macrophages from *Spp1* $^{KO/KO}$ mice compared with noise-
540 exposed WT mice, whereas expression of the apoptosis-related molecules caspase-8
541 and caspase-9 was not decreased (Fig. S5A–D). The WT and NE groups each comprised
542 three independently prepared single-cell samples (N = 3), whereas the *Spp1* $^{KO/KO}$
543 sample was prepared as a single pool of cochleae from eight mice (one biological
544 replicate), because each KO cochlear single-cell preparation requires pooling eight
545 animals (see Methods and Discussion).

546 ELISA analysis of cochlear protein lysates showed that IL-1β and IL-6 levels were
547 elevated after noise exposure in WT mice and that this increase was attenuated in *Spp1*
548 $^{KO/KO}$ mice (Fig. 7D, E). IL-18 showed a change in the same direction that did not reach
549 statistical significance (Fig. 7F). Analysis of key molecules in the pyroptosis pathway
550 [34-37] showed that *Spp1* knockout had no significant effect on the proportion of
551 macrophages expressing *Nlrp3*, *Gsdmd* or IL-1β; only the proportion of caspase-1^{+}
552 macrophages was markedly decreased after *Spp1* deletion under noise-exposure
553 conditions (Fig. S5E–I).

554 These data therefore associate SPP1 with an enhanced pyroptosis-associated
555 inflammatory signature in the noise-exposed cochlea, while direct evidence that these
556 macrophages undergo pyroptotic cell death remains to be established.

Genetic ablation of *Spp1* or *Ccr2* attenuates noise-induced hearing loss

Given the findings above that CCR2 mediates SPP1^{+} macrophage recruitment and that SPP1 deficiency dampens the inflammatory program of cochlear macrophages, we next assessed whether genetic ablation of *Ccr2* or *Spp1* could protect against noise-induced cochlear damage. Macrophages have been reported to participate in the repair and clearance of damaged synapses after noise exposure, and inflammatory factors released by macrophages may contribute to hair cell damage [10, 38, 39]. We therefore evaluated auditory threshold shifts, hair cell survival and ribbon-synapse integrity in noise-exposed WT, *Ccr2* $^{KO/KO}$ and *Spp1* $^{KO/KO}$ mice (Fig. 5). Baseline auditory function, assessed by ABR thresholds across frequencies, showed no significant differences between knockout and WT mice before noise exposure (Fig. 4B), and baseline hair cell counts were comparable across genotypes (Fig. 4A, C, D).

We exposed WT, *Spp1* $^{KO/KO}$ and *Ccr2* $^{KO/KO}$ mice to 110 dB SPL broadband noise. All mice were male (n = 6 per group), and auditory function was assessed longitudinally in the same cohort: ABR thresholds were recorded before noise exposure and again 14 days after exposure, so that each animal served as its own control. At 14 days post-exposure, both *Spp1* $^{KO/KO}$ and *Ccr2* $^{KO/KO}$ mice exhibited smaller ABR threshold shifts than WT mice (Fig. 5B); absolute threshold values (dB SPL) are reported in addition to threshold shifts (Fig. 4B and Fig. 5B). Immunofluorescence analysis of cochlear basilar membranes showed that *Ccr2* $^{KO/KO}$ mice retained more hair cells (Fig. 5A, C) and synapses (Fig. 5D, E) than WT controls after noise exposure, and that *Spp1* $^{KO/KO}$ mice

were protected to a comparable extent (Fig. 5A, C–E). We note that baseline synapse counts were slightly higher in *Spp1* $^{KO/KO}$ mice than in WT controls in the middle and basal turns (Fig. 4E); the genotype comparison was therefore made within a single exposure cohort, and a contribution of this baseline difference to the apparent magnitude of protection cannot be fully excluded.

Pharmacological inhibition of SPP1 or CCR2 attenuates noise-induced hearing loss

Although genetic knockout conferred significant protection against NIHL, global germline knockout cannot exclude developmental compensation. To further validate the effect of targeting SPP1 and CCR2, we performed pharmacological inhibition experiments in wild-type mice, administering SPP1 and CCR2 inhibitors by intraperitoneal injection, with a vehicle-treated control group (Fig. 8A). At 14 days post-noise, ABR threshold shifts were attenuated in both inhibitor-treated groups relative to the control (Fig. 8B). Consistent with the genetic findings, inhibitor-treated mice also showed better preservation of hair cells and synapses (Fig. 8C–F). These observations indicate that targeting SPP1 or CCR2 before noise exposure attenuates noise-induced hearing loss and cochlear damage.

Discussion

In this study, we identified a distinct SPP1^{+} macrophage subpopulation that expands in the cochlea at three days post-noise exposure and contributes to noise-induced hearing

599 loss (NIHL) pathology. Through integrated single-cell RNA sequencing, genetic
600 knockout models and pharmacological inhibition, we showed that these macrophages
601 are CCR2^{+} and negative for P2RY12, consistent with a monocyte-derived origin, and
602 that they accumulate in the cochlea following acoustic overstimulation. Functionally,
603 SPP1^{+} macrophages exhibited a pro-inflammatory state, as evidenced by the
604 upregulation of *Spp1*, *Fn1* and *Il1b* in the single-cell data. This pro-inflammatory state
605 was accompanied by an increased pyroptosis-associated signature, and cochlear IL-1β
606 and IL-6 levels were attenuated in *Spp1*-deficient mice, whereas IL-18 showed a non-
607 significant trend in the same direction. At single-cell resolution, only the proportion of
608 caspase-1^{+} macrophages was significantly reduced by *Spp1* knockout, whereas *Nlrp3*
609 and *Gsdmd* were unchanged (Fig. S5E–I). Because "proportion of" measures are
610 internally normalised to macrophage number, this selective reduction argues against the
611 lower cochlear IL-1β and IL-18 protein levels being attributable solely to a reduced
612 macrophage burden; the bulk ELISA measurements, however, report protein content of
613 whole-cochlear lysates and were therefore not adjusted for macrophage abundance.
614 Genetic ablation or pharmacological inhibition of SPP1 or CCR2 reduced noise-
615 induced auditory threshold shifts and preserved cochlear hair cells and ribbon synapses.
616 Collectively, these findings suggest that the SPP1–CCR2 axis coordinates the
617 recruitment and pro-inflammatory activation of a pathogenic macrophage subset,
618 positioning SPP1^{+} macrophages as a candidate target for preventive intervention in
619 NIHL, pending further validation.

While SPP1 has been detected in endolymph under steady-state conditions[16], our findings suggest its upregulation in macrophages and supporting cells following acoustic trauma, raising the possibility of a context-dependent functional shift. Elevated SPP1 expression has also been reported in age-related hearing loss[17], implying a potential role across different forms of hearing impairment. Building on a previous transcriptomic atlas[12], our study provides preliminary insights into a potential pathogenic $SPP1^{+}$ macrophage subset and its recruitment in NIHL, pending further mechanistic validation.

The gene signature observed in the $SPP1^{+}$ macrophage cluster, including *C1qa*, *C1qb*, *C1qc*, *Trem2*, *Spp1*, and *Apoe*, has been previously characterized as a disease-associated module[40]. In Alzheimer's disease models, SPP1 secreted by perivascular macrophages and fibroblasts mediates microglial phagocytosis of ApoE-labeled synaptic structures, a process in which complement component C1q plays a critical role[13]. Additionally, *MS4A7*, which was highly expressed in this cluster, has been reported to directly activate the NLRP3 inflammasome in macrophages, thereby exacerbating local inflammatory responses[41, 42]. The upregulation of *Il1b* and *Nlrp3* in macrophages after noise exposure, together with the differential IL-1β expression between $Spp1^{+}$ and $Spp1^{-}$ subsets, suggests that the $Spp1^{+}$ macrophage subpopulation may be involved in modulating pyroptosis-related pathways and may exert pro-inflammatory functions in response to noise, although this possibility requires further functional validation.

SPP1-expressing macrophages are increasingly recognized as a conserved, disease-associated macrophage state rather than a population unique to the inner ear. Cross-tissue integration of 235,930 macrophages from six human organs identified $SPP1^+$ macrophages as a shared feature of fibrosis, and resolved within them a further 'matrisome-associated' polarization state that emerges along their differentiation trajectory [43]. In skeletal muscle dystrophy, single-cell and spatial transcriptomics combined with functional assays showed that macrophage-derived *Spp1* directs the differentiation of stromal progenitors [44]. Our data place the cochlea within this framework: the *Spp1*-high macrophage cluster that emerges after acoustic trauma shares with those populations an enrichment of lysosomal and efferocytic programs, together with the capacity to engage neighboring cells through SPP1–CD44 and SPP1–integrin pairs (Fig. S2B). A parallel single-cell study of the noise-exposed and aging cochlea recently described a distinct pro-inflammatory $CD74^+CD14^+$ macrophage subset that expands in both conditions and shows enhanced communication with spiral ganglion neurons [10], reinforcing the view that cochlear macrophages constitute a heterogeneous compartment in which injury selects for functionally specialized, pro-inflammatory states. Within this literature, the distinctive contribution of the present work is the functional demonstration, using both genetic ablation and receptor/ligand-directed pharmacology, that the $SPP1^+$ state selected by acoustic trauma is coupled to threshold shift and cochlear synaptopathy, and that CCR2-dependent influx is required for it.

Cross-species relevance was assessed using a published single-cell atlas of the human inner ear (GSE213796) [21]. In that dataset, *Spp1* was also detected in non-immune compartments, including mesenchymal and epithelial cells that can give rise to cochlear structures such as the spiral ligament and supporting cells [45]. GSEA of expressed genes in both species indicated that human and murine $SPP1^+$ macrophages share enrichment of pathways related to responses to peptides and to inflammatory cytokine activation (Fig. S3C–E). These concordant signals support the existence of a

669 conserved SPP1^{+} macrophage state across species, although the small number of human
670 specimens limits how far this comparison can be taken.
671 The origin of cochlear macrophages after noise exposure remains debated. Macrophage
672 function and differentiation are closely linked to their origins[46]. Resident
673 macrophages in homeostatic tissues typically exert anti-inflammatory functions,
674 whereas recruited macrophages contribute to disease pathology in conditions such as
675 myocardial infarction and stroke[47, 48]. CCR2 is recognized as a marker for
676 monocyte-derived macrophages[18, 19, 49], while P2RY12 serves as a stable marker
677 for microglia[50, 51]. Our observation that SPP1^{+} macrophages are predominantly
678 CCR2^{+} and negative for P2RY12, together with the absence of Mki67 induction in these
679 cells (Fig. 6G), raises the possibility that these cells originate from peripheral
680 monocytes rather than local proliferation. Using *Ccr2*$^{RFP/+}$ *Cx3cr1*$^{GFP/+}$ dual-reporter
681 mice, Pan et al.[6] reported that tissue-resident macrophages dominate the cochlear
682 response to noise and contribute to hair cell damage. In contrast, our findings are
683 consistent with a predominantly monocyte-derived, CCR2^{+} origin of the expanded
684 SPP1^{+} macrophage population. This discrepancy may reflect differences in noise
685 exposure paradigms, mouse strains, or the specific macrophage subsets analyzed. Our
686 observation that CCR2 knockout reduces both the number of SPP1^{+} macrophages and
687 noise-induced hearing loss further supports a functional role for monocyte-derived
688 macrophages in NIHL pathology, consistent with studies implicating CCR2 signaling
689 in monocyte recruitment across various inflammatory conditions[19, 47, 52].
690 Our finding that *Ccr2* ablation protects against noise-induced threshold shift and

ribbon-synapse loss appears to differ from an earlier report in which *Ccr2*-deficient mice on a CX3CR1+/GFP background showed no change in monocyte recruitment into the cochlea and, paradoxically, increased noise-induced hair cell death after octave-band noise at 112 dB [53]. Three considerations reconcile these observations. First, the two paradigms interrogate different segments of the injury continuum: octave-band exposure at 112 dB produces overt hair cell loss, whereas the broadband (2–20 kHz) exposure used here leaves the sensory epithelium largely intact and manifests predominantly as synaptic and functional injury. Second, the genetic backgrounds differ: in the CX3CR1+/GFP reporter strain one *Cx3cr1* allele is replaced by GFP, itself a modification of macrophage biology, whereas the present experiments used a constitutive *Ccr2* null allele on a uniform C57BL/6J background. Third, the two studies measured different cellular endpoints: the earlier work quantified the total number of cochlear macrophages and found no difference, whereas in our data the decrease in the proportion of $SPP1^+$ macrophages (Fig. 6C) was markedly greater than the accompanying change in overall macrophage proportion (Fig. 6B); the protection we observe therefore reflects a shift in the composition of the macrophage compartment rather than a wholesale reduction in macrophage abundance. Because the earlier study also reported greater hair cell loss in *Ccr2*-deficient mice, whereas we observed improved outer hair cell survival in the basal turn (Fig. 5A, C), the most parsimonious reading is that CCR2-dependent recruitment is context-dependent, with the recruited cells becoming net pathogenic under a paradigm dominated by synaptic and functional injury. Whether this reflects compartment-specific actions of a single receptor or strain- and paradigm-dependent differences is an empirical question rather than a logical contradiction, and could be addressed by macrophage-restricted *Ccr2* deletion combined with an SPP1 reporter across a gradient of noise intensities.

CellChat analysis predicted that $SPP1^+$ macrophages participate in frequent communication with other cochlear cell types after noise exposure, notably through the

718 SPP1–CD44 and SPP1–ITGAV/ITGB1 axes. These predictions are consistent with
719 findings in other pathological contexts. For instance, SPP1^{+} tumor-associated
720 macrophages have been shown to remodel the tumor microenvironment through SPP1–
721 CD44 interactions [54], and SPP1^{+} macrophages have been shown to define a distinct
722 macrophage state that coordinates cellular programs across multiple cell types in the
723 tumor microenvironment, influencing disease progression and patient outcomes [55].
724 Collectively, these observations raise the possibility that SPP1^{+} macrophages contribute
725 to intercellular communication in cochlear inflammation, a prediction that requires
726 experimental validation.
727 We found that pyroptosis- and inflammation-associated markers, including caspase-1,
728 IL-1β and IL-6, were increased after noise exposure and were attenuated in *Spp1*-
729 deficient mice, whereas IL-18 showed a trend in the same direction that did not reach
730 statistical significance. These observations raise the possibility that *Spp1* contributes to
731 inflammatory activation of cochlear macrophages in the noise-exposed cochlea. Similar
732 associations between tissue injury and pyroptosis have been reported in other contexts
733 [56-58], but the present data do not establish that *Spp1* drives macrophage pyroptotic
734 cell death, nor do they address how the released mediators contribute to tissue
735 inflammation.
736 Similar links between phagocytosis and inflammatory cell death have been reported in
737 other contexts, where excessive efferocytosis triggers caspase-dependent inflammatory
738 signaling and IL-1β maturation; in our dataset this raises the hypothesis that the

efferocytic program of SPP1^{+} macrophages contributes to their inflammatory state, which remains to be tested directly. NLRP3 inflammasome activation in cochlear macrophages has also been implicated in NIHL and other auditory pathologies [6, 26, 59], supporting a pathogenic role for macrophage inflammasome activation. We also observed that *Spp1* deficiency reduced the pro-inflammatory molecule *Fn1* and the recruitment-associated receptor *Ccr2* in cochlear macrophages after noise exposure, whereas *Mif* and *Lgals9* were not reduced in the same direction, indicating that SPP1 influences the macrophage phenotype rather than uniformly suppressing it. Consistent with this, *Trem2*, a key immune surveillance molecule [6, 60], was upregulated after noise exposure and was slightly but significantly reduced in *Spp1* $^{KO/KO}$ mice, although the levels remained above the unexposed baseline, suggesting that SPP1 contributes to the homeostatic-to-pro-inflammatory shift. Our finding that *Tyrobp*, a phagocytosis-associated adaptor that forms a signaling complex with TREM2, was differentially regulated after *Spp1* knockout suggests a potential interplay between SPP1 and TYROBP signaling in cochlear macrophages. This is consistent with a previous study showing that long-term running exercise upregulates both SPP1 and TYROBP expression in the hippocampus of APP/PS1 mice, accompanied by enhanced microglial metabolic activity and morphological plasticity [61].

The upregulation of *Il1b* and *Nlrp3* in cochlear macrophages after acoustic trauma is corroborated by an independent single-cell analysis of 97,043 cochlear cells showing that macrophage NLRP3 inflammasome activation accounts for circadian variation in NIHL severity, and that pharmacological NLRP3 inhibition preserves ribbon synapses

761 [59]. Of note, *Spp1* deletion in our hands reduced the proportion of caspase-1^{+}
762 macrophages and attenuated cochlear IL-1β and IL-6 protein levels, with a non-
763 significant trend for IL-18 (Fig. 7D–F) without detectable changes in *Nlrp3* or *Gsdmd*
764 transcript abundance (Fig. S5E-I). We therefore do not interpret SPP1 as a
765 transcriptional inducer of inflammasome components; rather, these data are compatible
766 with SPP1 acting upstream of, or parallel to, inflammasome assembly, for example by
767 licensing the recruited cells for an IL-1β-high state or by sustaining their retention in
768 the injured sensory epithelium. Because mature IL-1β release is governed by post-
769 translational caspase-1 processing, transcript-level measurements cannot distinguish
770 these alternatives, and direct readouts of inflammasome activation—cleaved GSDMD,
771 ASC speck formation, or IL-1β secretion assays in sorted macrophages—are required
772 to resolve them.

773 Several limitations should be acknowledged. First, we used systemic germline
774 knockout and pharmacological inhibitors, which do not allow cell-type-specific
775 conclusions; conditional knockout models are needed to validate the macrophage-
776 intrinsic roles of SPP1 and CCR2. Second, CellChat predictions of ligand–receptor
777 interactions require experimental validation, for example using neutralizing antibodies
778 or genetic disruption. Third, direct evidence of macrophage pyroptosis, such as cleaved
779 GSDMD or ASC speck formation, is lacking. Fourth, the scRNA-seq dataset (105 dB)
780 and the functional experiments (110 dB) used different noise paradigms, warranting
781 cautious interpretation when integrating these datasets. Fifth, some single-cell
782 comparisons were based on a limited number of biological replicates. In particular,
783 because the immune-cell yield of a single mouse cochlea is very low, each cochlear
784 single-cell preparation requires pooling cochleae from eight animals; whereas the WT

785 and noise-exposed (NE) groups each comprised three independently prepared pools,
786 the *Spp1* $^{KO/KO}$ single-cell group represents only one such pool and could not be repeated
787 three times within the scope of this study. The scRNA-seq findings obtained from this
788 group (Fig. S5A-I) should therefore be regarded as descriptive, and although they are
789 internally consistent with the ELISA and histological results obtained from
790 independently replicated experiments, they will require confirmation in additional
791 independently prepared KO samples. The sample size (N) for each group is now stated
792 in the corresponding figure legends. Sixth, only male mice were used, and sex is an
793 established biological variable in both immune responses and susceptibility to noise-
794 induced hearing loss; whether the protective effects of *Spp1* or *Ccr2* ablation described
795 here generalize to female mice remains to be determined. Seventh, the discovery-stage
796 single-cell analysis is constrained by cell numbers: the re-analyzed public dataset
797 (GSE167078) yielded only 96 cochlear macrophages in total, of which 27, 46, 13 and
798 10 were recovered at baseline, 3dNE, 7dNE and 14dNE, respectively. All cluster-level
799 comparisons—including the Cluster 10/11 compositional shift that underpins our
800 central hypothesis—therefore rest on small numbers of cells, and the confidence
801 intervals around the reported proportions are correspondingly wide; the same
802 consideration applies to the pathway analysis, which was performed on a restricted
803 input gene set (n = 35). Eighth, single-cell suspensions necessarily discard spatial
804 information, so the physical proximity of SPP1^{+} macrophages to hair cells, ribbon
805 synapses and spiral ganglion neurons is inferred from immunofluorescence rather than

quantified in situ; spatial transcriptomics or high-dimensional imaging will be required to define the cellular neighborhoods in which SPP1 signaling actually operates, since juxtacrine relationships cannot be established from transcriptional prediction alone. Ninth, the human observations derive from a very small number of inner ear specimens spanning widely different developmental stages, and the cross-species correlation with the murine dataset is weak (R = 0.22, Fig. S3F); these data support the existence of $SPP1^{+}$ macrophages in the human inner ear but do not establish that the mechanism described here operates in human NIHL. Tenth, cochlear drug exposure was not measured directly for the inhibitors used in Fig. 8, so the pharmacological arm is presented as corroborative rather than as independent proof of target engagement. Eleventh, both pharmacological inhibitors were administered before and during the exposure period; the present design therefore demonstrates a preventive effect, and efficacy with post-exposure initiation of treatment remains to be established. Addressing these limitations—particularly macrophage-restricted genetic deletion, direct inflammasome readouts, and spatially resolved validation—will help determine whether the SPP1–CCR2 axis identified here is a causal driver of NIHL or a marker of the injury-associated macrophage response.

Conclusions

Our findings show that genetic ablation or pharmacological inhibition of SPP1 and CCR2 attenuates noise-induced hearing loss and cochlear damage, supporting a functional role for these molecules in NIHL. The protective effects observed in *Ccr2*

$^{KO/KO}$ mice are consistent with the established role of CCR2 in monocyte recruitment across inflammatory conditions [19, 47, 62]. Because both inhibitors were administered before and during the exposure period, these pharmacological experiments demonstrate a preventive rather than a therapeutic effect; whether SPP1 or CCR2 blockade retains efficacy when initiated after noise exposure remains to be tested. The value of modulating macrophage function in hearing loss is further supported by recent work showing that inhibition of TLR4 signaling in cochlear macrophages alleviates noise-induced damage [6]. Together with our results, these findings suggest that targeting the SPP1–CCR2 axis may represent a viable preventive strategy for auditory injury.

Declarations

Ethics approval and consent to participate

All animal procedures were approved by the Institutional Animal Care and Use Committee (IACUC) of Air Force Medical University (approval no. IACUC-20260039) and were conducted in accordance with the ARRIVE 2.0 guidelines and the NIH Guide for the Care and Use of Laboratory Animals. No new human subjects or human tissue samples were collected for this study; the only human data analysed were publicly available, de-identified single-nucleus RNA-sequencing data (GSE213796).

Consent for publication

Not applicable.

Data availability

The RNA-sequencing data generated during the current study are available in the GEO repository, https://www.ncbi.nlm.nih.gov/geo/query/acc.cgi?acc=GSE346691. The public datasets re-analysed in the current study are available in the GEO repository, https://www.ncbi.nlm.nih.gov/geo/query/acc.cgi?acc=GSE167078 and https://www.ncbi.nlm.nih.gov/geo/query/acc.cgi?acc=GSE213796.

Competing interests

The authors declare that they have no competing interests.

Funding

This work was supported by the National Natural Science Foundation of China (82571312 to D.J.Z, 82301303 to B.F, 82401349 to Y.Y).

Author contributions

Z.Q.W., X.Y.Z., and M.H.Q. contributed equally to this article. Z.Q.W. performed the laboratory experiments. D.J.Z., J.C., and X.C.W. designed this study. X.Y.Z., M.H.Q., and P.Z. contributed to the mouse audiology tests. Z.J.G., X.Y.Z., X.Y.D., and Z.Q.W. contributed to the data analysis. Z.Q.W. and X.Y.Z. contributed to the animal support for the study. Z.Q.W. and X.Y.Z. suggested changes to the figures. Z.Q.W., D.J.Z., and J.C. contributed to critical discussions. Z.Q.W. wrote the paper. All the authors read and approved the final manuscript.

Acknowledgements

The authors thank Wuhan Igenebook Genome Sequencing Company for providing RNA-sequencing technical support, Cyagen (Suzhou) Biosciences for generating the *Spp1* KO/KO mice, and Wuhan Youdu Biotechnology (Wuhan, China) for providing the *Ccr2* KO/KO mice.

Abbreviations

ABR: auditory brainstem response; ANOVA: analysis of variance; CCR2: C-C motif chemokine receptor 2; ELISA: enzyme-linked immunosorbent assay; GEO: Gene Expression Omnibus; GSDMD: gasdermin D; IL: interleukin; KO: knockout; NIHL:

noise-induced hearing loss; NK: natural killer; NLRP3: NOD-, LRR- and pyrin domain-containing 3; SPP1: secreted phosphoprotein 1; scRNA-seq: single-cell RNA sequencing; SEM: standard error of the mean; t-SNE: t-distributed stochastic neighbour embedding; UMAP: uniform manifold approximation and projection; WT: wild-type

Additional files

Additional file 1: Supplementary Figures S1–S5. Fig. S1: marker-gene dot plot and source-associated molecular heat map; Fig. S2: CellChat cell–cell communication analysis; Fig. S3: human inner-ear single-cell dataset (GSE213796); Fig. S4: hair-cell and ribbon-synapse staining with auditory brainstem responses in wild-type mice; Fig. S5: macrophage subset proportions in *Spp1* KO/KO mice. Each figure is presented with its complete legend. (PDF)

Additional file 2: Uncropped western blot membranes underlying Fig. 2D, with molecular-weight markers and lane assignments. (DOCX)

References

1. Chadha S, Kamenov K, Cieza A. The world report on hearing, 2021. Bull World Health Organ. 2021;99(4):242–2A.

2. Feng B, Dong T, Song X, Zheng X, Jin C, Cheng Z, et al. Personalized Porous Gelatin Methacryloyl Sustained-Release Nicotinamide Protects Against Noise-Induced Hearing Loss. Adv Sci (Weinh). 2024;11(12):e2305682.

3. Xu K, Xu B, Gu J, Wang X, Yu D, Chen Y. Intrinsic mechanism and pharmacologic treatments of noise-induced hearing loss. Theranostics. 2023;13(11):3524–49.

4. Okano T, Nakagawa T, Kita T, Kada S, Yoshimoto M, Nakahata T, et al. Bone marrow-derived cells expressing Iba1 are constitutively present as resident tissue macrophages in the mouse cochlea. J Neurosci Res. 2008;86(8):1758–67.

5. Yang W, Vethanayagam RR, Dong Y, Cai Q, Hu BH. Activation of the antigen presentation function of mononuclear phagocyte populations associated with the basilar membrane of the cochlea after acoustic overstimulation. Neuroscience. 2015;303:1–15.

6. Pan J, Wang K, Qu J, Chen D, Chen A, You Y, et al. Activated tissue-resident macrophages contribute to hair cell insults in noise-induced hearing loss in mice. Commun Biol. 2024;7(1):1078.

7. Sung CYW, Hayase N, Yuen PST, Lee J, Fernandez K, Hu X, et al. Macrophage depletion protects against cisplatin-induced ototoxicity and nephrotoxicity. Sci Adv. 2024;10(30):eadk9878.

8. Song X, Li Y, Guo R, Yu Q, Liu S, Teng Q, et al. Cochlear resident macrophage mediates development of ribbon synapses via CX3CR1/CX3CL1 axis. Front Mol Neurosci. 2022;15:1031278.

9. Yi Y, Wu M-Y, Chen K-T, Chen A-H, Li L-Q, Xiong Q, et al. LDHA-mediated glycolysis in stria vascularis endothelial cells regulates macrophages function through CX3CL1-CX3CR1 pathway in noise-induced oxidative stress. Cell Death Dis. 2025;16(1):65.

10. Wu M-Y, Chen A-H, Li L-Q, Yi Y, Xiong Q, Chen K-T, et al. Single-cell RNA sequencing analysis of mouse cochlea identifies a novel proinflammatory CD74+CD14+ macrophage subset in mice with age-related and noise-induced hearing loss. Hear Res. 2025;466:109376.

11. Murali SV, Stothert AR, Pereyra E, Batalkina L, Kaur T. CX3CR1 fate mapping in vivo distinguishes cochlear resident and recruited macrophages after acoustic trauma. Front Immunol. 2025;16:1678176.

12. Milon B, Shulman ED, So KS, Cederroth CR, Lipford EL, Sperber M, et al. A cell-type-specific atlas of the inner ear transcriptional response to acoustic trauma. Cell Rep. 2021;36(13):109758.

13. De Schepper S, Ge JZ, Sierksma A, Crowley G, Ferreira LSS, Garceau D, Toomey CE, et al. Perivascular cells induce microglial phagocytic states and synaptic engulfment via SPP1 in mouse models of Alzheimer's disease. Nat Neurosci. 2023;26(3):406–15.

14. Morse C, Tabib T, Sembrat J, Buschur KL, Bittar HT, Valenzi E, et al. Proliferating SPP1/MERTK-expressing macrophages in idiopathic pulmonary fibrosis. Eur Respir J. 2019;54(2):1802441.

15. Han H, Ge X, Komakula SSB, Desert R, Das S, Song Z, et al. Macrophage-derived Osteopontin (SPP1) Protects From Nonalcoholic Steatohepatitis. Gastroenterology. 2023;165(1):201–17.

16. Fukuda M, Okanishi H, Ino D, Ono K, Ota T, Wakai E, et al. Protein profile of mouse endolymph suggests a role in controlling cochlear homeostasis. iScience. 2024;27(11):111214.

17. Yuan Y, Zhang J, Zhao J, Zhang X, Cao Z. Expression of ApoE and Spp1 in the cochlea and auditory cortex of age-related hearing loss mice. Braz J Otorhinolaryngol. 2025;91(6):101674.

18. Georgakis MK, Bernhagen J, Heitman LH, Weber C, Dichgans M. Targeting the CCL2-CCR2 axis for atheroprotection. Eur Heart J. 2022;43(19):1799–808.

19. Hulsmans M, Schloss MJ, Lee IH, Bapat A, Iwamoto Y, Vinegoni C, et al. Recruited macrophages elicit atrial fibrillation. Science. 2023;381(6654):231–9.

20. Al-Qazazi R, Lima PDA, Prisco SZ, Potus F, Dasgupta A, Chen K-H, et al. Macrophage-NLRP3 Activation Promotes Right Ventricle Failure in Pulmonary Arterial Hypertension. Am J Respir Crit Care Med. 2022;206(5):608–24.

21. van der Valk WH, van Beelen ESA, Steinhart MR, Nist-Lund C, Osorio D, de Groot JCMJ, et al. A single-cell level comparison of human inner ear organoids with the human cochlea and vestibular organs. Cell Rep. 2023;42(6):112623.

22. Jin S, Guerrero-Juarez CF, Zhang L, Chang I, Ramos R, Kuan CH, et al. Inference and analysis of cell-cell communication using CellChat. Nat Commun. 2021;12:1088.

23. Fernandez DM, Rahman AH, Fernandez NF, Chudnovskiy A, Amir E-aD, Amadori L, et al. Single-cell immune landscape of human atherosclerotic plaques. Nat Med. 2019;25(10):1576–88.

24. Li X, Li S, Wang Y, Zhou X, Wang F, Muhammad I, et al. Single cell RNA-sequencing delineates CD8(+) tissue resident memory T cells maintaining rejection in liver transplantation. Theranostics. 2024;14(12):4844–60.

25. Chen B, Sun Y, Sun H, Cong N, Ma R, Qian X, et al. Ultrasound-Triggered NO Release to Promote Axonal Regeneration for Noise-Induced Hearing Loss Therapy. ACS Nano. 2024;18(48):33232–44.

26. Qi M, Gao Z, Qiu Y, Wang R, Tian K, Yue B, et al. NOX2 Contributes to High-Frequency Outer Hair Cell Vulnerability in the Cochlea. Adv Sci (Weinh). 2025;12(34):e08830.

27. Ouyang Q, Wang C, Sang T, Tong Y, Zhang J, Chen Y, et al. Depleting profibrotic macrophages using bioactivated in vivo assembly peptides ameliorates kidney fibrosis. Cell Mol Immunol. 2024;21(8):826–41.

28. Hoeft K, Schaefer GJL, Kim H, Schumacher D, Bleckwehl T, Long Q, et al. Platelet-instructed SPP1+ macrophages drive myofibroblast activation in fibrosis in a CXCL4-dependent manner. Cell Rep. 2023;42(2):112131.

29. Wang J, Wang S, Ren L, Liu X, Zhang L, Hu P, et al. Targeting Itga8 Mitigates Neurogenic Bladder Fibrosis Driven by Trem2^{+} Macrophage-Derived Fn1 via FAK/RhoA/ROCK Signaling. Adv Sci (Weinh). 2026;13(9):e10631.

30. Sumaiya K, Langford D, Natarajaseenivasan K, Shanmughapriya S. Macrophage migration inhibitory factor (MIF): A multifaceted cytokine regulated by genetic and physiological strategies. Pharmacol Ther. 2022;233:108024.

31. Zeng L, Hu P, Zhang Y, Li M, Zhao Y, Li S, et al. Macrophage migration inhibitor factor (MIF): Potential role in cognitive impairment disorders. Cytokine Growth Factor Rev. 2024;77:67–75.

32. Li Y, Sang Y, Chang Y, Xu C, Lin Y, Zhang Y, et al. A Galectin-9-Driven CD11chigh Decidual Macrophage Subset Suppresses Uterine Vascular Remodeling in Preeclampsia. Circulation. 2024;149(21):1670–88.

33. Fan G, Tao C, Li L, Xie T, Tang L, Han X, et al. The co-location of MARCO+ tumor-associated macrophages and CTSE+ tumor cells determined the poor prognosis in intrahepatic cholangiocarcinoma. Hepatology. 2025;82(1):25–41.

34. Yu P, Zhang X, Liu N, Tang L, Peng C, Chen X. Pyroptosis: mechanisms and diseases. Signal Transduct Target Ther. 2021;6(1):128.

35. Liu Y, Pan R, Ouyang Y, Gu W, Xiao T, Yang H, et al. Pyroptosis in health and disease: mechanisms, regulation and clinical perspective. Signal Transduct Target Ther. 2024;9(1):245.

36. Elias EE, Lyons B, Muruve DA. Gasdermins and pyroptosis in the kidney. Nat Rev Nephrol. 2023;19(5):337–50.

37. Zhang Z, Zhang Y, Xia S, Kong Q, Li S, Liu X, et al. Gasdermin E suppresses tumour growth by activating anti-tumour immunity. Nature. 2020;579(7799):415–20.

38. Manickam V, Gawande DY, Stothert AR, Clayman AC, Batalkina L, Warchol ME, et al. Macrophages Promote Repair of Inner Hair Cell Ribbon Synapses following Noise-Induced Cochlear Synaptopathy. J Neurosci. 2023;43(12):2075–89.

39. Jin S, Kim SJ, Lyu A-R, Shin S-A, Kim TH, Jin L, et al. Metabolic-dysfunction-associated steatohepatitis impairs cochlear integrity and delays auditory recovery after noise trauma. Cell Commun Signal. 2026;24(1):222.

40. Li H, Miao Y, Zhong L, Feng S, Xu Y, Tang L, et al. Identification of TREM2-positive tumor-associated macrophages in esophageal squamous cell carcinoma:

implication for poor prognosis and immunotherapy modulation. Front Immunol. 2023;14:1162032.

41. He Y, Hara H, Nunez G. Mechanism and Regulation of NLRP3 Inflammasome Activation. Trends Biochem Sci. 2016;41(12):1012–21.

42. Zhou L, Qiu X, Meng Z, Liu T, Chen Z, Zhang P, et al. Hepatic danger signaling triggers TREM2(+) macrophage induction and drives steatohepatitis via MS4A7-dependent inflammasome activation. Sci Transl Med. 2024;16(738):eadk1866.

43. Ouyang JF, Mishra K, Xie Y, Park H, Huang KY, Petretto E, et al. Systems level identification of a matrisome-associated macrophage polarisation state in multi-organ fibrosis. eLife. 2023;12:e85530.

44. Coulis G, Jaime D, Guerrero-Juarez CF, Kastenschmidt JM, Farahat PK, Nguyen Q, et al. Single-cell and spatial transcriptomics identify a macrophage population associated with skeletal muscle fibrosis. Sci Adv. 2023;9(27):eadd9984.

45. Kolla L, Kelly MC, Mann ZF, Anaya-Rocha A, Ellis K, Lemons A, et al. Characterization of the development of the mouse cochlear epithelium at the single cell level. Nat Commun. 2020;11(1):2389.

46. Lazarov T, Juarez-Carreno S, Cox N, Geissmann F. Physiology and diseases of tissue-resident macrophages. Nature. 2023;618(7966):698–707.

47. Park MD, Silvin A, Ginhoux F, Merad M. Macrophages in health and disease. Cell. 2022;185(23):4259–79.

48. Sanin DE, Ge Y, Marinkovic E, Kabat AM, Castoldi A, Caputa G, et al. A common framework of monocyte-derived macrophage activation. Sci Immunol. 2022;7(70):eabl7482.

49. Rizzo G, Gropper J, Piollet M, Vafadarnejad E, Rizakou A, Bandi SR, et al. Dynamics of monocyte-derived macrophage diversity in experimental myocardial infarction. Cardiovasc Res. 2023;119(3):772–85.

50. Kenkhuis B, Somarakis A, Kleindouwel LRT, van Roon-Mom WMC, Hollt T, van der Weerd L. Co-expression patterns of microglia markers Iba1, TMEM119 and P2RY12 in Alzheimer's disease. Neurobiol Dis. 2022;167:105684.

51. Butovsky O, Jedrychowski MP, Moore CS, Cialic R, Lanser AJ, Gabriely G, et al. Identification of a unique TGF-β-dependent molecular and functional signature in microglia. Nat Neurosci. 2014;17(1):131–43.

52. Dick SA, Wong A, Hamidzada H, Nejat S, Nechanitzky R, Vohra S, et al. Three tissue resident macrophage subsets coexist across organs with conserved origins and life cycles. Sci Immunol. 2022;7(67):eabf7777.

53. Sautter NB, Shick EH, Ransohoff RM, Charo IF, Hirose K. CC chemokine receptor 2 is protective against noise-induced hair cell death: studies in CX3CR1+/GFP mice. J Assoc Res Otolaryngol. 2006;7(4):361–72.

54. Dong L, Hu S, Li X, Pei S, Jin L, Zhang L, et al. SPP1(+) TAM Regulates the Metastatic Colonization of CXCR4(+) Metastasis-Associated Tumor Cells by Remodeling the Lymph Node Microenvironment. Adv Sci (Weinh). 2024;11(44):e2400524.

55. Bill R, Wirapati P, Messemaker M, Roh W, Zitti B, Duval F, et al. CXCL9:SPP1 macrophage polarity identifies a network of cellular programs that control human cancers. Science. 2023;381(6657):515–24.

56. Zhang Y, Zhang L, Xu H, Yin X, Zheng X, Cui N, et al. Severe fever with thrombocytopenia syndrome virus infection of the male reproductive tract induces pathology and inflammation. Nat Microbiol. 2026;11(5):1286–301.

57. Li B, Liu J, He W, Zhou Y, Zhao M, Xia C, et al. Inhibition of macrophage inflammasome assembly and pyroptosis with GC-1 ameliorates acute lung injury. Theranostics. 2025;15(6):2360–74.

58. Ma J, Wang Y, Xu W, Wang H, Wan Z, Guo J. Macrophage pyroptosis in atherosclerosis: therapeutic potential. Acta Biochim Biophys Sin (Shanghai). 2025;57(6):857–70.

59. Ma Q, Wang Q, Zhu Z, Zhou Q, Wang Z, Qian M, et al. Single-Cell Sequencing Reveals Circadian Sensitivity of Noise-Induced Hearing Loss Mediated by Macrophage-Driven NLRP3 Inflammasome Activation. Neurosci Bull. 2026;42(2):319–37.

60. Kleinberger G, Yamanishi Y, Suarez-Calvet M, Czirr E, Lohmann E, Cuyvers E, et al. TREM2 mutations implicated in neurodegeneration impair cell surface transport and phagocytosis. Sci Transl Med. 2014;6(243):243ra86.

61. Zhang SS, Zhu L, Peng Y, Zhang L, Chao FL, Jiang L, et al. Long-term running exercise improves cognitive function and promotes microglial glucose metabolism and morphological plasticity in the hippocampus of APP/PS1 mice. J Neuroinflammation. 2022;19(1):34.

62. Krenkel O, Puengel T, Govaere O, Abdallah AT, Mossanen JC, Kohlhepp M, et al. Therapeutic inhibition of inflammatory monocyte recruitment reduces steatohepatitis and liver fibrosis. Hepatology. 2018;67(4):1270–83.

Figures:

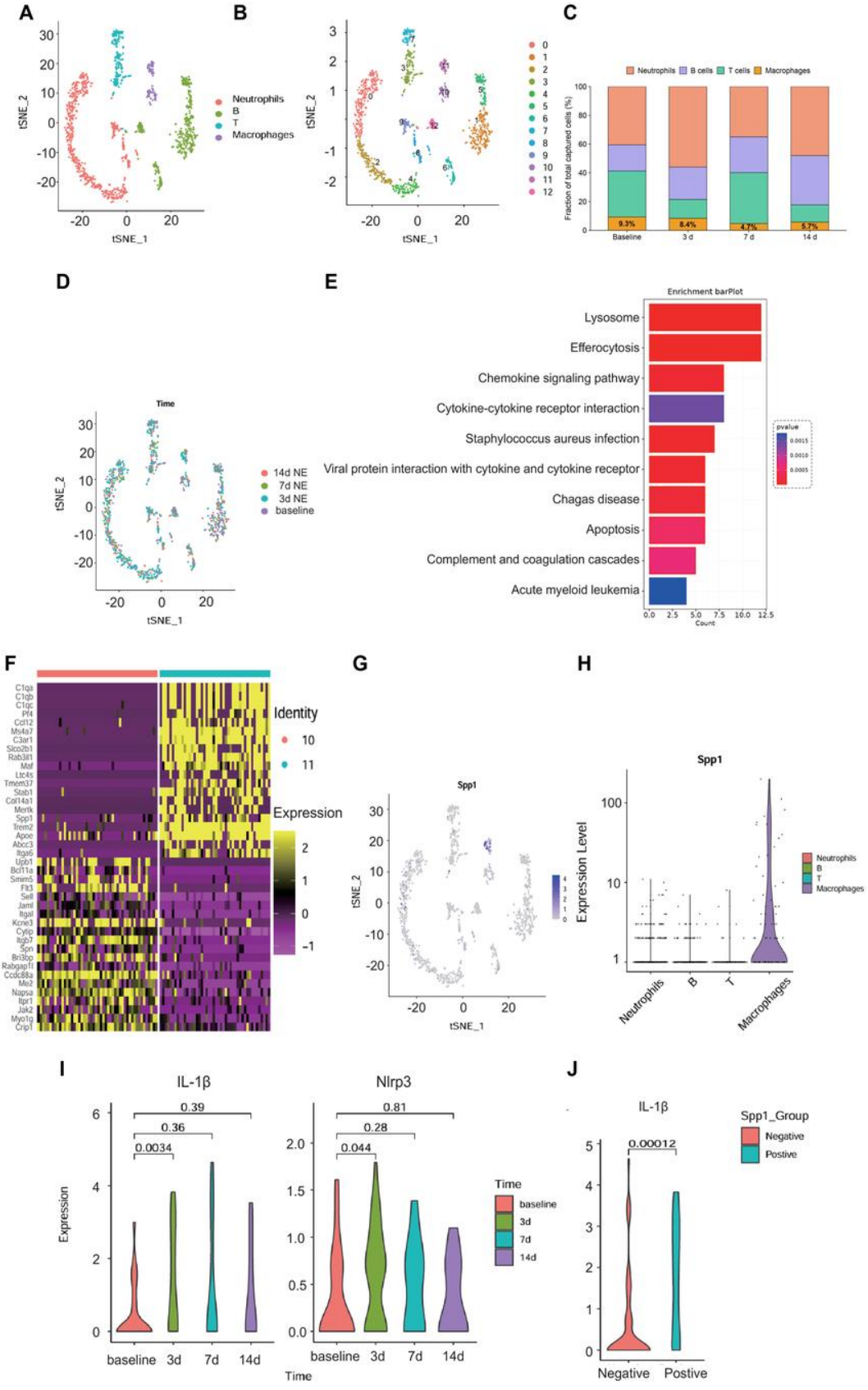

Fig. 1. Emergence of an *Spp1*-highly expressing macrophage subset at three days

post-noise exposure. (A) t-SNE clustering and cell type annotation of cochlear immune cells, showing major populations including neutrophils, T cells, B cells, and macrophages. (B) t-SNE plot of the same cells coloured by cluster, revealing a total of 13 immune cell clusters (designated 0–12), with clusters 10 and 11 identified as macrophages. (C) Stacked bar chart showing the normalized cellular composition of recovered cochlear immune cells at each time point; the macrophage fraction (Clusters 10 and 11 combined) is indicated within each bar. (D) t-SNE plot of cochlear immune cells coloured by time point (baseline, 3dNE, 7dNE, 14dNE). Cross-tabulation of cluster identity (B) with time point showed that macrophages at three days post-noise exposure were predominantly cluster 11 (63.0% versus 22.2% at baseline; Fisher's exact test P = 0.0014). (E) KEGG pathway enrichment analysis of differentially expressed genes in cluster 11 macrophages, showing enrichment of gene sets associated with lysosomal activation, efferocytosis, Staphylococcus aureus infection and monocyte recruitment. The corresponding cluster 10 pathways (cell adhesion molecules, adjusted P = 0.0067; PI3K–Akt signaling, adjusted P = 0.024) are reported in the main text and are not displayed in this panel. (F) Heatmap showing differentially expressed genes between clusters 10 and 11. The *Spp1*-highly expressing macrophage subset exhibited significantly upregulated expression of phagocytosis-related molecules. (G) t-SNE plot showing *Spp1* expression distribution. (H) *Spp1* expression was specifically elevated in macrophages. (I) Expression of the inflammasome components *Il1b* and *Nlrp3* in macrophages at the indicated times after noise exposure. (J) IL-1β expression levels differed significantly between $Spp1^{+}$ and $Spp1^{-}$ macrophages.

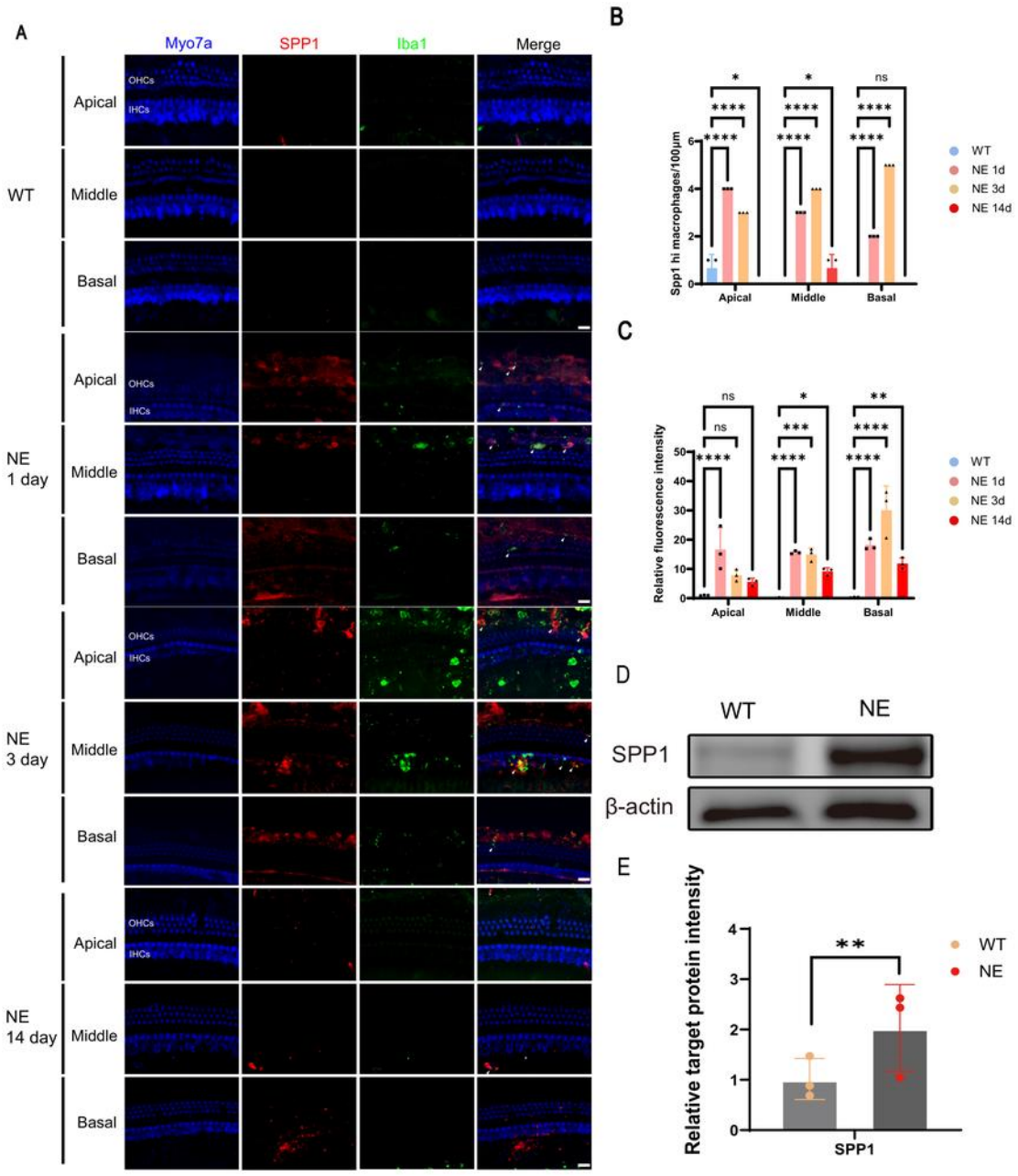

Fig. 2. SPP1^{+} macrophages increase after noise exposure. (A) Immunofluorescence staining of cochlear basilar membrane whole mounts before noise exposure and at 1 day, 3 days, and 14 days post-noise exposure, showing SPP1 (red), Iba1 (macrophage marker), and *Myo7a* (hair cell marker). Representative images; scale bar = 10 μm. (B) Quantification of SPP1-highly expressing macrophages from the images shown in (A) (n = 3). (C) Quantitative analysis of relative SPP1 fluorescence intensity from the

images shown in (A) (n = 3). In (B) and (C), bar identity is indicated by colour: WT = light blue, NE 1 d = pink, NE 3 d = orange, NE 14 d = red. (D, E) Western blot analysis of SPP1 protein in mouse cochlear lysates at 3 days post-noise exposure. Band intensities were quantified and normalised to β-actin for fold-change calculation. (D) Representative blots; the two lanes shown were cropped from Blot 1 (left lane, R3, unexposed control; right lane, R2, 110 dB day 3). (E) Quantification from n = 3 independent experiments; individual data points shown; data are mean ± SEM; unpaired two-tailed Student's t-test. Full-length uncropped membranes, with molecular-weight markers (Vazyme MP201; 180, 130, 100, 70, 55, 40, 35, 25, 20, 15 and 12 kDa), lane assignments and a calibrated kDa scale for each membrane, are provided in the supplementary uncropped-blot file; the lanes cropped for (D) are marked by red rectangles in that file. ns, not significant; *$p < 0.05$; **$p < 0.01$; ***$p < 0.001$; ****$p < 0.0001$.

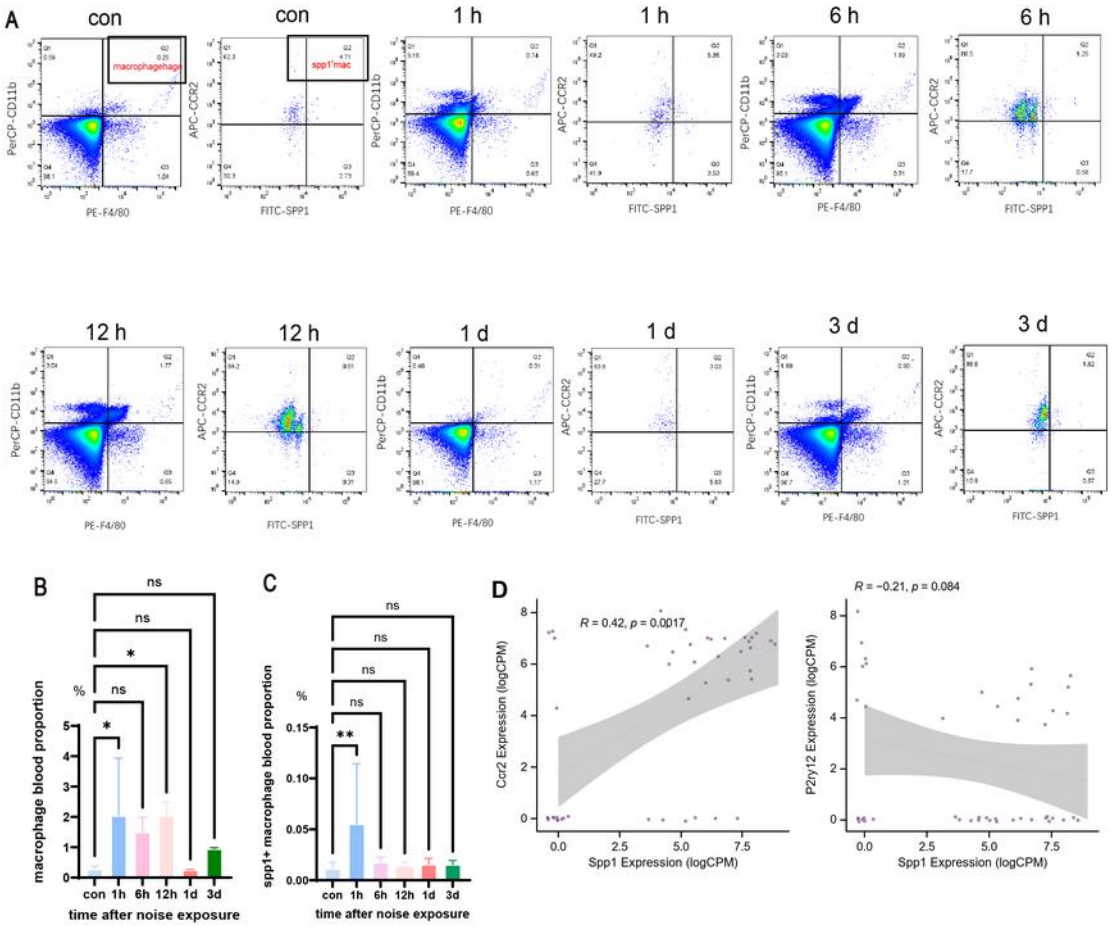

Fig. 3. CCR2 signaling mediates the increase of SPP1$^+$ macrophages after noise exposure. (A) Flow cytometric quantification of blood macrophages (CD11b$^+$F4/80$^+$) and SPP1$^+$ macrophages (CD11b$^+$F4/80$^+$CCR2$^+$SPP1$^+$) in C57BL/6J mice before noise exposure and at 1 h, 6 h, 12 h, 1 d, and 3 d post-noise exposure (n = 3, from three independent experiments). (B) Quantitative analysis of blood macrophages from the data shown in (A). (C) Quantitative analysis of blood SPP1$^+$ macrophages from the data shown in (A). ns, not significant; *p < 0.05; **p < 0.01. (D) Correlation between *Spp1* and *Ccr2* (left) and between *Spp1* and *P2ry12* (right) expression in individual macrophages from the noise-exposed cochlea (GSE167078), computed across all macrophages without pre-selecting *Spp1*$^+$ cells. Each dot represents one cell (n = 46

cells); the shaded band indicates the 95% confidence interval of the linear fit; R and P values were obtained by Spearman's rank correlation.

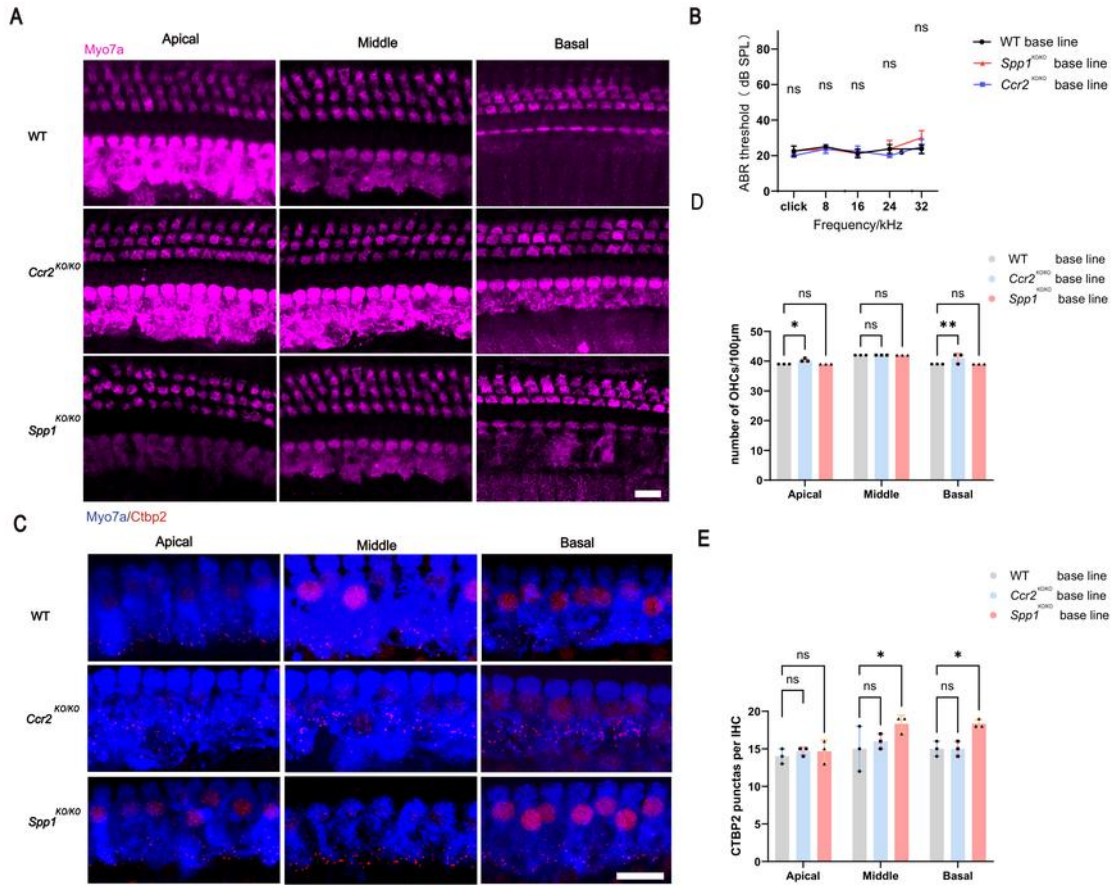

Fig. 4. Baseline hearing thresholds and immunofluorescence staining of hair cells and synapses in *Ccr2* $^{KO/KO}$ and *Spp1* $^{KO/KO}$ mice before noise exposure. (A) Immunofluorescence staining of cochlear hair cells (*Myo7a*) in the apical, middle, and basal turns of wild-type, *Ccr2* $^{KO/KO}$, and *Spp1* $^{KO/KO}$ mice before noise exposure. (B) Baseline ABR thresholds in wild-type, *Ccr2* $^{KO/KO}$, and *Spp1* $^{KO/KO}$ mice before noise exposure (n = 6). (C) Immunofluorescence staining of inner hair cells (*Myo7a*) and synapses (CtBP2) in the apical, middle, and basal turns of wild-type, *Ccr2* $^{KO/KO}$, and *Spp1* $^{KO/KO}$ mice before noise exposure. Scale bars = 10 μm (A, C). (D) Quantification of hair cell counts from the images shown in (A). No significant hair cell loss was observed in the three groups, and no statistically significant difference was found in hair cell counts (n = 3). (E) Quantification of synapse counts from the images shown in (C). No significant synapse loss was detected in any of the three groups. In *Spp1* $^{KO/KO}$

mice, synapse counts in the middle and basal turns were slightly higher than those in the other two groups (n = 3). In (D) and (E), bar identity is indicated by colour: WT = grey, *Ccr2* $^{KO/KO}$ = light blue, *Spp1* $^{KO/KO}$ = pink. ns, not significant; *p < 0.05.

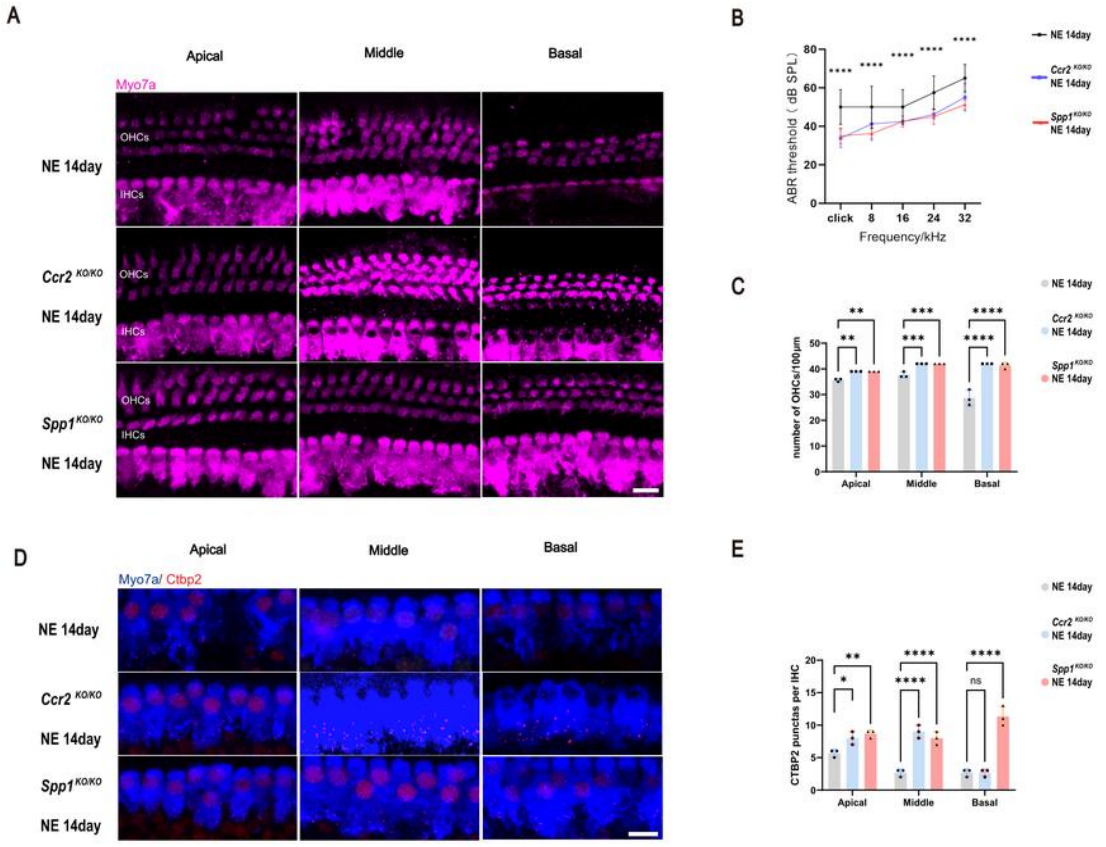

Fig. 5. Protective effects of *Ccr2* and *Spp1* knockout against noise-induced hearing loss. (A) Immunofluorescence staining of cochlear hair cells (*Myo7a*) in the apical, middle, and basal turns of wild-type, *Ccr2* $^{KO/KO}$, and *Spp1* $^{KO/KO}$ mice at 14 days post-noise exposure. (B) ABR thresholds in wild-type, *Ccr2* $^{KO/KO}$, and *Spp1* $^{KO/KO}$ mice 14 days after noise exposure. ABRs were elicited by click and pure-tone stimuli at 8, 16,

24, and 32 kHz (n = 6 mice per group; only male mice were used). The data are longitudinal, obtained from the same cohort of mice before (baseline) and 14 days after noise exposure, with each animal serving as its own baseline control; both absolute thresholds (dB SPL) and threshold shifts are shown. (C) Quantification of hair cell counts from the images shown in (A). After noise exposure, hair cell survival was higher in both *Ccr2* $^{KO/KO}$ and *Spp1* $^{KO/KO}$ mice than in WT controls (n = 3). (D) Immunofluorescence staining of inner hair cells (*Myo7a*) and synapses (CtBP2) in the apical, middle, and basal turns of wild-type, *Ccr2* $^{KO/KO}$, and *Spp1* $^{KO/KO}$ mice at 14 days post-noise exposure. Scale bars = 10 μm (A, D). (E) Quantification of synapse counts from the images shown in (D). After noise exposure, synapse numbers were higher in *Spp1* $^{KO/KO}$ mice than in WT controls in all three turns, and higher in *Ccr2* $^{KO/KO}$ mice in the apical and middle turns (n = 3). In (C) and (E), bar identity is indicated by colour: WT NE = grey, *Ccr2* $^{KO/KO}$ NE = light blue, *Spp1* $^{KO/KO}$ NE = pink. ns, not significant; **$p < 0.01$; ****$p < 0.0001$.

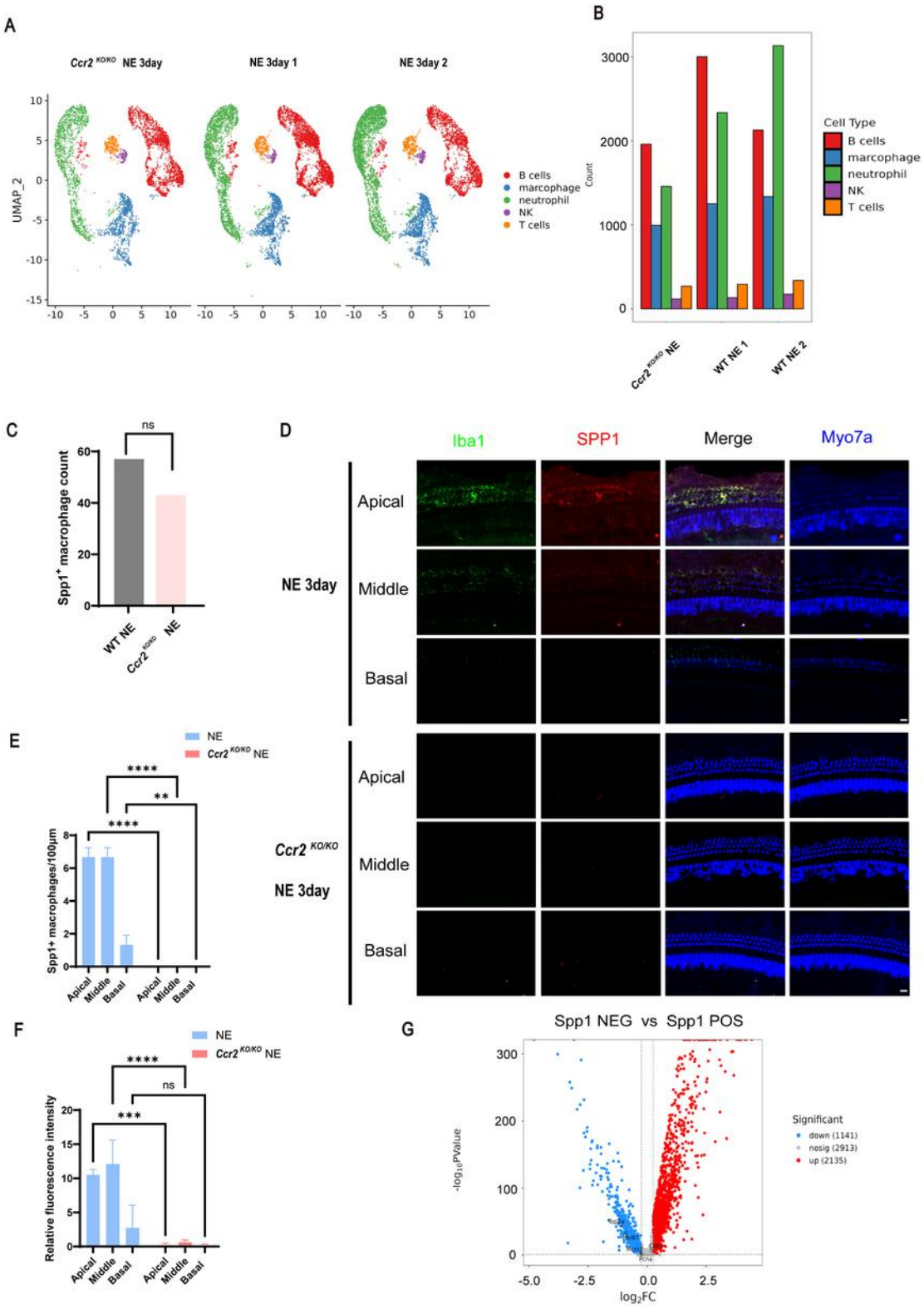

Fig. 6. *Ccr2* knockout leads to a reduction in SPP1⁺ macrophages recruited after

noise exposure. (A) UMAP clustering and cell type annotation of cochlear immune cells. (B) Bar plot illustrating the normalized cellular composition (proportion of total recovered cells) of cochlear immune populations in noise-exposed *Ccr2* $^{KO/KO}$ mice and two independent biological replicates of noise-exposed wild-type samples (WT-NE1 and WT-NE2); CCR2 knockout reduced the numbers of recovered macrophages and neutrophils. (C) Number of SPP1^{+} macrophages in the single-cell data from *Ccr2* KO/KO and wild-type mice at 3 days post-noise exposure (bars colour-coded: WT NE = grey; *Ccr2* KO/KO NE = light pink); the difference was not statistically significant. (D) Immunofluorescence staining of Iba1, SPP1, and *Myo7a* at 3 days post-noise exposure in WT and *Ccr2* $^{KO/KO}$ mice. Scale bar = 10 μm (D). (E) Quantification of SPP1^{+} macrophage density (cells per 100 μm) in the apical, middle, and basal turns of wild-type and *Ccr2* $^{KO/KO}$ mice at 3 days post-noise exposure (n = 4). (F) Relative SPP1 fluorescence intensity in the apical, middle, and basal turns of WT and *Ccr2* KO/KO mice at 3 days post-noise exposure (n = 4). In (E) and (F), bar identity is indicated by colour: NE = light blue and *Ccr2* $^{KO/KO}$ NE = pink. (G) Volcano plot (x-axis, $\log_2$ fold change; y-axis, $-\log_{10}$ adjusted P). Red and blue dots indicate genes significantly upregulated (n = 2135) or downregulated (n = 1141) in SPP1-positive versus SPP1-negative macrophages (|$\log_2$FC| > 1, adjusted P < 0.05); grey dots are non-significant. Five proliferation-related genes (Top2a, Mki67, Mcm2, Pcna, Cdk4) are labelled and lie within the non-significant region. ns, not significant; **p < 0.01; ***p < 0.001; ****p < 0.0001.

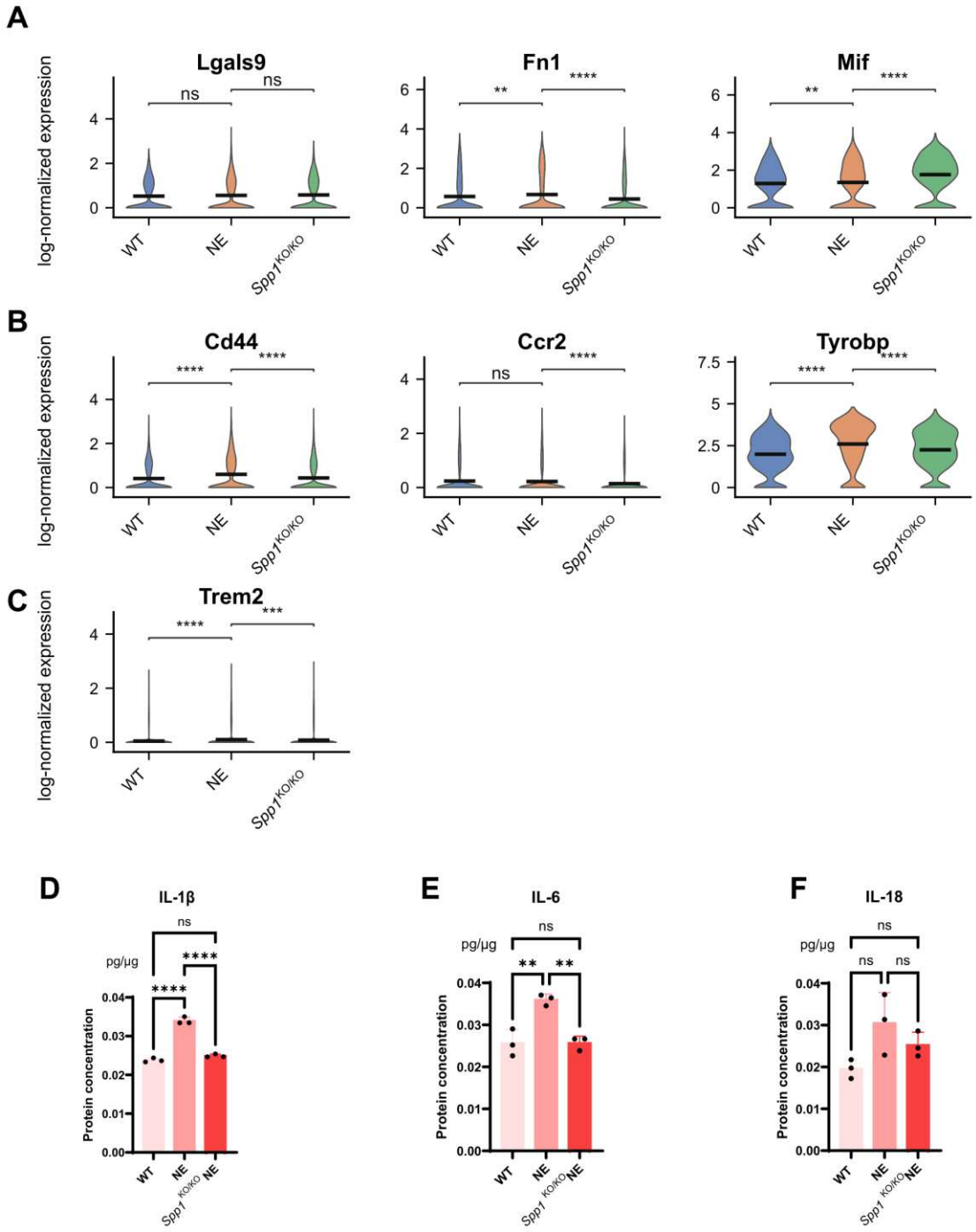

Fig. 7. *Spp1* mediates pro-inflammatory and receptor expression changes in cochlear macrophages, and *Spp1* knockout attenuates noise-induced pyroptosis-associated inflammation. (A–C) Single-cell RNA sequencing analysis of the monocyte–macrophage lineage population (annotated as 'Monocytes' in the integrated dataset (GSE346691; 14,039 cells across the three groups)). (A) Violin plots of macrophage pro-inflammatory gene expression (*Lgals9*, *Fn1* and *Mif*; log-transformed

normalized counts). (B) Violin plots of macrophage receptor expression (Cd44, *Ccr2* and Tyrobp). (C) Violin plot of macrophage *Trem2* expression. In (A–C), the three groups — WT (no noise), NE (wild-type mice 3 days post-noise) and *Spp1* $^{KO/KO}$ (*Spp1* knockout mice 3 days post-noise) — are shown side by side in a single panel per gene; the horizontal bar in each violin indicates the mean. Statistical significance was determined using the two-sided Wilcoxon rank-sum test. (D–F) Protein levels of IL-1β, IL-6 and IL-18 in cochlear lysates from the same three groups (ELISA). ns, not significant; *$p < 0.05$; **$p < 0.01$; ***$p < 0.001$; ****$p < 0.0001$. IL-1β and IL-6 were elevated after noise exposure and attenuated in *Spp1* $^{KO/KO}$ mice, whereas IL-18 showed a similar trend that did not reach statistical significance.

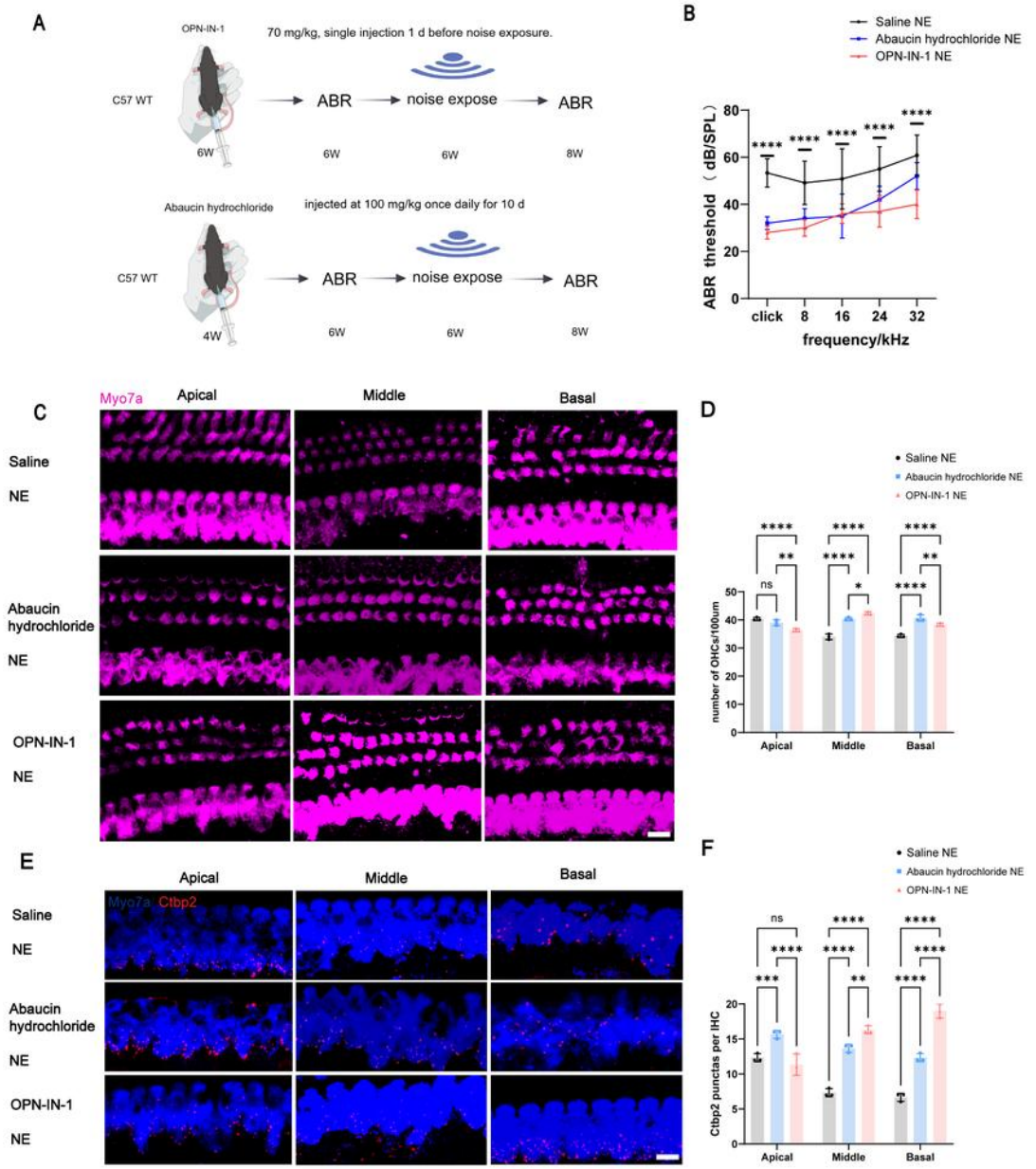

Fig. 8. Hair cell and synapse staining and auditory threshold shifts after noise exposure following administration of SPP1 and CCR2 inhibitors. (A) Dosing regimen and administration schedule of the SPP1 inhibitor (MCE HY-146064) and the CCR2 inhibitor (MCE HY-18611). (B) ABR thresholds of the three groups of mice (saline + NE, SPP1 inhibitor + NE, CCR2 inhibitor + NE) at click, 8, 16, 24, and 32

kHz. SPP1 and CCR2 inhibitors significantly reduced noise-induced increases in hearing thresholds (n = 6). (C) Immunofluorescence staining of cochlear hair cells (*Myo7a*) in the apical, middle, and basal turns of saline-, SPP1-inhibitor- and CCR2-inhibitor-treated mice before and after noise exposure. (D) Quantification of hair cell counts from the images shown in (C). The two inhibitors showed a protective effect on hair cells after noise exposure (n = 3). (E) Immunofluorescence staining of inner hair cells (*Myo7a*) and synapses (CtBP2) in the apical, middle, and basal turns of saline-, SPP1-inhibitor- and CCR2-inhibitor-treated mice before and after noise exposure. Scale bars = 10 μm (C, E). (F) Quantification of synapse counts from the images shown in (E). The two inhibitors showed a protective effect on synapses after noise exposure (n = 3). ns, not significant; ***$p < 0.001$; ****$p < 0.0001$.

Supplementary Files

This is a list of supplementary files associated with this preprint. Click to download.

- Additionalfile1SupplementaryFiguresS1S5.pdf
- SupplementaryDatauncroppedWBmembranes.docx